Design and Prototyping of an Integrated Powered Hip and Microprocessor-Controlled Knee Unit for Hip-Knee-Ankle-Foot Prostheses

Yousef Bader

Thesis submitted to the Faculty of Engineering
in partial fulfillment of the requirements for the degree of

MASTER OF APPLIED SCIENCE

In Biomedical Engineering

Ottawa-Carleton Institute for Biomedical Engineering
University of Ottawa
Ottawa, Ontario

May 2023

Abstract

Hip-knee-ankle-foot (HKAF) prostheses are full lower limb devices for people with hip amputations. They are designed to enable individuals to regain their mobility and move freely with little restriction. HKAFs typically have high rejection rates among users, as well as gait asymmetry and increased trunk anterior-posterior lean and pelvic tilt. In this thesis, a novel integrated hip-knee (IHK) unit was designed and evaluated to address the limitations of existing solutions. This IHK combines powered hip and microprocessor controlled knee joints into one structure, with shared electronics, sensors, and batteries. The unit is also adjustable to the user leg length by a prosthetist. ISO-10328 standard mechanical testing demonstrated acceptable structural safety and rigidity. Successful functional testing involved three able-bodied participants walking with the IHK in a hip prosthesis simulator. Hip and knee joint angles and pelvic tilt angles were recorded, gait characteristics were analyzed using video recordings. Testing showed that the participants were able to walk using the IHK, and data showed that participants used different walking strategies. Points of improvement were identified for future development of the thigh unit, including completion of a synergistic gait control system, improved battery holding mechanism, and amputee user testing.

Table of Contents

List of Figures

List of Tables

Abbreviations

2MWT	2-Minute Walk Test
ADC	Analog-to-digital converter
HD	Hip disarticulation
HKAF	Hip-knee-ankle-foot
HP	Hemipelvectomy
IHK	Integrated hip knee
LCI/LCII	Load condition I / Load condition II
MPC	Microprocessor-controlled
RMSE	Root mean square error
ROM	Range of motion

Acknowledgements

I'd like to first thank my two supervisors, Dr. Edward Lemaire and Dr. Natalie Baddour for their guidance, support, encouragement, and help in the completion of my thesis. I would like to thank Mitacs for funding this research.

I'd also like to acknowledge and thank the following individuals:

Staff of Össur
David Langlois

Research team at The Ottawa Hospital Rehabilitation Center
Farshad Golshan
Hossein Gholizadeh
Sarah Mroz
Kelly Lynn Hill Brannen
Michael Botros

I'd also like to thank my family and friends for supporting me throughout all the ups and downs of my research.

Chapter 1: Introduction

1.1 Overview

People with hip disarticulation (HD: full amputation of the lower limb) and hemipelvectomy (HP: full amputation of the lower limb and partial amputation of the pelvis) have the option of using a hip-knee-ankle-foot (HKAF) prosthesis to move within their environment. HKAF prostheses are the most complex type of lower-limb prostheses because they must include hip, knee, ankle, and foot components that can fit and function together to enable the user to move freely with little restriction.

While HKAF prostheses have the potential to enable amputees to regain their mobility, one in three HKAF prostheses are rejected by their user [1], [2]. Common HKAF rejection reasons include slow walking speed, need for secondary walking aids [1], prosthesis weight [3], difficulty of use [3], and increased energy expenditure [4] of using a prosthesis compared to using a wheelchair.

Recent prosthesis development has focused on reducing prosthesis rejection rates by integrating microprocessors and sensors to offer adaptive devices that adjust in real-time to achieve optimal walking conditions. These microprocessor-controlled (MPC) prostheses include passive joints that use variable damping to control joint acceleration/deceleration [5] or active joints that use electric motors to provide torque to help with energy-intensive tasks such as step-over-step stair climbing and standing from a sitting position [6]. People who transitioned from mechanical knee prostheses to MPC knee prostheses showed improved balance and stability [7], as well as increased daily activity and increased satisfaction in daily life [8].

Several commercial non-MPC hip prostheses are available; however, commercial MPC prostheses are not available for people with HD and HP amputations. One of the most advanced non-MPC prostheses is the Ottobock Helix3D hip joint, a mechanical hip joint designed for HD and HP amputees. Walking speed improved for level-ground, uphill, and downhill stair descent when amputees had their prostheses upgraded to a the Helix3D hip joint [1], [9]. Furthermore, walking aid use was reduced after people became acclimated with the Helix-C-leg knee prosthesis, which is designed for use with the Helix3D [1]. The

Helix3D is an improvement for HD and HP amputees, however there is still room for improvement in hip prosthesis design. People using non-MPC mechanical hip prostheses expend on average three times more energy and move at less than half the speed of hip amputees using wheelchairs [4], leading to complaints of fatigue after long periods of prosthesis use.

In this thesis, a new active MPC hip-knee-ankle-foot prosthesis was designed and evaluated. The new device integrated a powered MPC hip joint (developed at the Ottawa Hospital Research Institute and uOttawa) with a passive MPC knee based on the Össur Rheo Knee 3 to provide coordinated electronic control and shared electronic resources for a compact, all-in-one solution for lower limb HD or HP amputees (Integrated Hip-Knee unit; IHK).

1.2 Rationale

Locomotion is a fundamental part of everyday life. In urban environments, people walk on average 6500 steps per day at a speed of approximately 1.3 m/s [10]. Lower limb amputations hinder a person's ability to move and participate in daily activities. 90% of all amputations are related to the lower limb [10] and 44,430 lower limb amputations were reported in Canada between 2006 and 2011 (22.9 per 100,000, with 24.9% knee disarticulation or transfemoral amputations and 0.7% hip and pelvis amputations) [11]. While the relative number of HD and HP amputations is small, people with this amputation level have many additional challenges for appropriate mobility.

The availability of commercial and research prostheses reflects the lower limb amputation incidence rates, with a variety of state-of-the-art MPC knee prosthesis options [6], [10] but no commercially available MPC hip prostheses and only one MPC research hip device [12]. The lack of viable MPC options for hip amputees supports the need to develop new MPC hip prostheses, because switching from mechanical devices to MPC devices improves gait for ankle [13], knee [7], and hip [1], [9] compared to mechanical joints.

MPC devices provide advanced control over joint motion. Sensor data can be used to determine user state and intent recognition algorithms allow automatic and smooth transitions between level ground, ramp ascent and descent, and stair modes. Modern MPC

knee prostheses offer manual mode switching that allows the user to change device settings based on their activities, such as exercising and cycling. MPC devices can improve user safety with stumble recovery functions that can detect and mitigate potentially dangerous motions and minimize harm to the user [6].

An active MPC hip device would allow for better swing initiation and control and would allow the leg to be lifted higher when walking on slopes. A mechanical hip joint requires excessive hip and trunk motion to swing forward [9]. With an active hip prosthesis, the trunk and pelvis will not need to compensate for lack of torque applied at the hip.

Ideally, new MPC hip devices would integrate a MPC knee to enable resource sharing such as, sensor data, battery power, and processing power between the two joints. Shared sensors and processing could enable multi-joint coordination for potentially improved gait, sit-to-stand motion, and mobility in the community. Currently, the hip and knee joints work independently with no synergistic control. Additionally, all knee components could be moved into the thigh instead of the shank. This will shift the limb weight distribution above the knee joint and closer to the hip joint, reducing required joint actuator torque during swing. This would also bring all electronic components into the thigh, eliminating the need for wires running across the knee joint.

1.3 Objectives

The objective of this thesis is to develop and evaluate a thigh component for a powered hip-knee-ankle-foot prosthesis. This Integrated Hip Knee (IHK) unit includes a powered hip joint, microprocessor-controlled knee joint (Össur Rheo Knee 3), and all sensors, electronics, and battery.

1.4 Thesis contributions

In this thesis, a novel prosthetic thigh component was created that integrates a new powered hip joint, an Össur Rheo Knee 3, sensors, battery, and electronics into one unit that is adaptable to the user and configurable by the prosthetist. The scope of this research was mechanical development and testing of the structural component of a prosthetic thigh and the mechanical connections to a powered hip joint and the Rheo Knee 3. The powered

hip joint, electronics, and software were developed by other members of the research team. The contributions of this research also include:

- A new approach to hip-level prosthetic systems that provides the benefits of powered mobility and microprocessor controlled movement but also can lead to synergistic hip and knee control since both joints share sensors, electronics, and gait intent algorithm control to coordinate the two joints during movement.
- Device evaluation according to ISO-10328 standard mechanical testing and demonstrated acceptable structural safety and rigidity.
- Research demonstrating that the Össur Rheo Knee 3 could work with sensor signals from the thigh and knee (typically shank and knee), thereby being a viable option for future iterations.
- The device underwent successful functional testing with three able-bodied participants. This process also demonstrated the viability of a new hip prosthesis simulator for initial evaluation of powered prostheses.

1.5 Thesis outline

This thesis is divided into six chapters. Chapter 2 provides a literature review of hip amputations, prosthetic solutions, and non-amputee and amputee gait. Chapter 3 discusses the design and development of the thigh unit. This chapter outlines the design criteria, summarizes the components, the assembly of the thigh unit, and user adjustability options, and includes the calculations and simulation results used to reach the final design. Chapter 4 discusses the methodology used to conduct the mechanical testing of the thigh unit and presents bench test results. Chapter 5 presents the methodology and results of walking tests. Chapter 6 summarizes the thesis and presents future work and improvements for the next iteration of the thigh unit.

Chapter 2: Literature Review

This chapter provides a review of the literature on hip-level amputations, walking gait characteristics, and available hip or knee prostheses. Section 2.1 provides a brief review of hip disarticulation and hemipelvectomy amputations. Section 2.2 provides a review of commercial and research prostheses. Section 2.3 provides an overview of able-bodied gait and discusses the effects of amputation on walking, as well as the effects of using different prostheses on walking. Section 2.4 provides a brief summary of amputee and non-amputee level ground walking gait. Section 2.5 provides a summary of the main conclusions of the literature review.

2.1 Hip amputations

Lower limb rehabilitation becomes more difficult as the amputation location nears the hip, with the most difficult cases being amputations that involve the entire lower limb (Figure 2.1) [1]. Hip amputations fall into two categories: hip disarticulation with amputation at the hip joint and hemipelvectomy with partial amputation of the pelvis [14]. In developed countries, the majority of lower limb amputations are performed on people over 60 years of age and are mostly caused by diabetes and vascular disease [11], [14], [15]. In contrast, in developing countries hip amputations are more likely to be performed on younger people and are commonly performed due to trauma, vascular insufficiency, femoral osteomyelitis, decubitus, failed hip arthroplasty, or congenital abnormality [14].

Hip disarticulation and hemipelvectomy incidence rates are relatively low. In Canada, between 2006 and 2011, 44,430 lower limb amputations were reported in ten provinces, with 309 (0.7%) hip and pelvis amputations [11]. In Germany, between 2005 and 2015, 322,330 lower limb amputations were reported, of which 339 (0.1%) were hemipelvectomy [15].

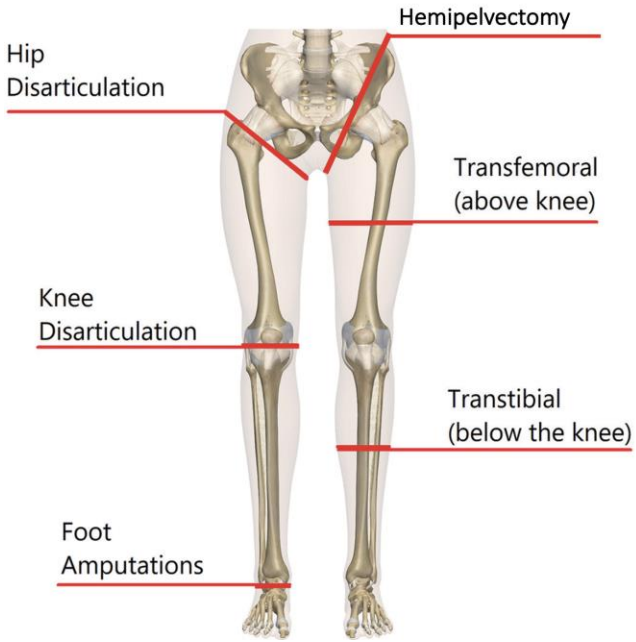

Figure 2.1 Levels of lower limb amputations (modified from [16])

Approximately one third of hip amputees reject their prostheses [3], with reasons including excessive device weight, preference for using a wheelchair, and the requirement of using a walker resulting in the inability to use their hands while standing. Fernández et al. [2] showed that younger users were more likely to accept their prosthesis, and people who accepted their prosthesis used their device for an average of 12.5 hours per day.

2.2 Hip-knee-ankle-foot prostheses

2.2.1 Post-WWI hip-knee-ankle-foot prostheses and the Canadian prosthesis

In the early 1900s, research into developing new and more effective HKAF prostheses increased because of post-WWI amputees. These prostheses featured metal, wood, and leather construction, resulting in relatively heavy devices. Additionally, due to the lack of plastics manufacturing at the time, the prosthesis socket was made of wood, leather, or metal, further contributing to the high device weight. Early HKAF designs used a monocentric (single point of rotation) locking hip joint that limited range of motion (ROM) when the locking mechanism was engaged and the person was walking. To sit down, the lock would be disengaged to allow the hip joint to freely flex to a sitting position [17].

With the development of plastics manufacturing in the 1950s, new devices were produced that replaced the heavier components, such as the socket, with light-weight reinforced plastic, greatly reducing prosthesis weight [17]. One such example is the Canadian prosthesis (Figure 2.2), developed in 1954 in Toronto by Colin McLaurin, and later improved by James Foort [18]. The Canadian prosthesis introduced several new design elements that improved upon previous designs:

- The hip joint was moved anterior and distal to the anatomical hip joint. The joint contacts the socket if it extends too far, allowing the socket to act as an extension limiter. This provided additional stability to the prosthesis [17], [18]. This change also made sitting more comfortable for the user since the hip joint hardware is not beneath the user.
- The locking hip joint was replaced with a freely moving monocentric hip joint with limiters. A nylon cord was used to limit hip flexion when walking. This cord needed to be unhooked for sitting [17].
- An elastic band was attached from the socket to just below the knee joint. This elastic band had the main function of resisting hip flexion while walking, and also providing the user some control over the knee joint [17].
- A rubber stop on the socket limited joint hyper-extension and also provided energy return to assist with swing [18].

While the Canadian prosthesis provided benefits and improvements to the HKAF prostheses of its time, this device still had problems that led to user rejection. One study reported that only one third of users fitted with a Canadian prosthesis continued to use their prosthesis after an 8 year follow up, with many people either moving to more modern options or rejecting hip prostheses in favour of crutches [2]. One of the main reasons for rejection of the Canadian prosthesis was ambulation difficulty and lumbar pain caused by the use of lumbar muscles to move the prosthesis [2], [3]. Other reasons included socket discomfort [2], [3] and excessive prosthesis weight [3].

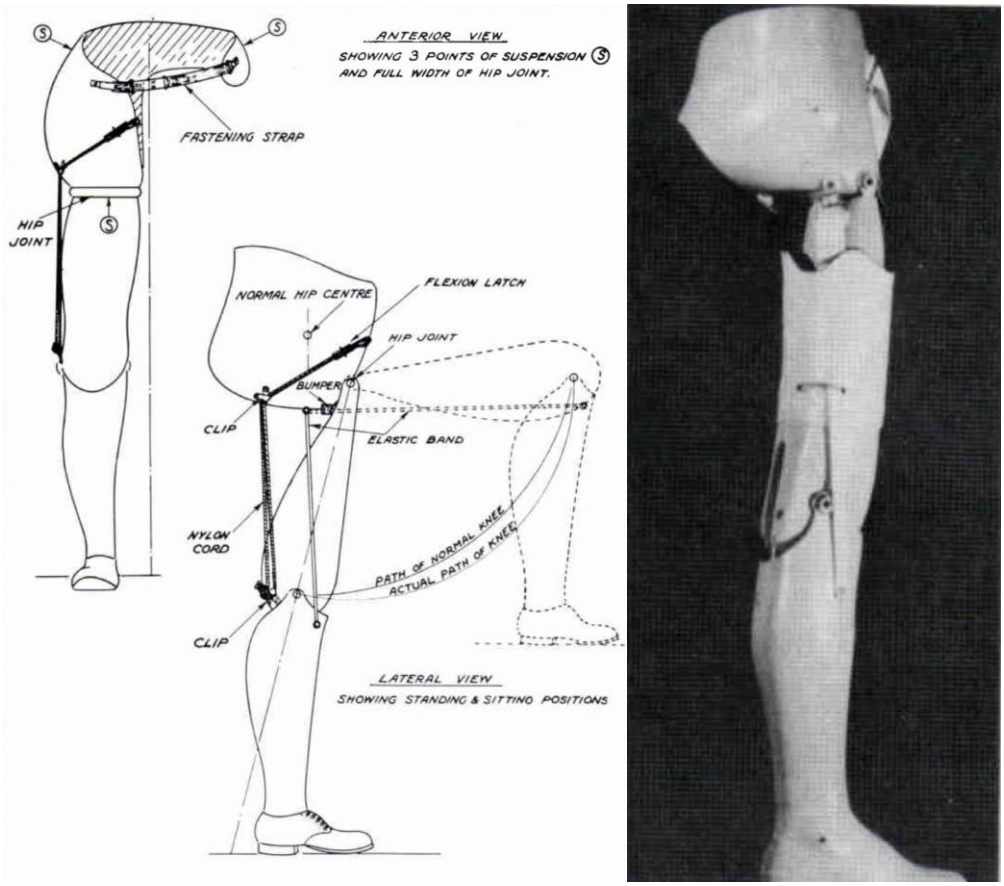

Figure 2.2 Canadian prosthesis schematics showing the elastic band nylon cord that limited range of motion (left) [17] and the actual construction (right) [3].

2.2.2 Ottobock 7E5 modular prosthetic hip joint

The Ottobock 7E5 is a monocentric locking hip joint that limits hip ROM while walking. The joint is located below the anatomical hip joint and has an adjustable ROM when the locking mechanism is engaged for walking. The manufacturer recommends using a knee joint from the same brand; however, the 7E5 can be used with other off-the-shelf knee joints. The 7E5 is only recommended for indoor mobility [19].

Figure 2.3 Ottobock 7E5 hip joint [19] (Copyright Ottobock).

2.2.3 Ottobock 7E7 modular prosthetic hip joint

The Ottobock 7E7 (Figure 2.4 left) is a mechanical joint for hip disarticulation and hemipelvectomy amputees that improves upon several of the features introduced by the Canadian prosthesis. This includes a free moving monocentric hip joint [9], [18] positioned anterior and distal to the anatomical hip joint, a rubber stopper to limit hyper-extension, and a spring (instead of an elastic band) to resist flexion and provide energy storage and return [18]. The 7E7 allows the prosthetist to align the joint such that it also acts in the transverse and frontal planes instead of only the sagittal plane (Figure 2.4 middle and right).

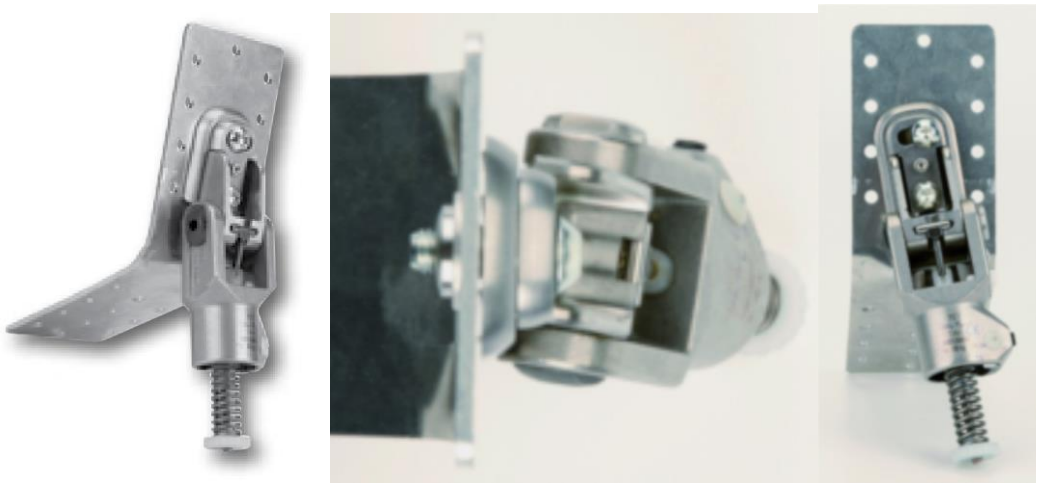

Figure 2.4 Ottobock 7E7 hip joint (left) [20]. The 7E7 can be aligned in the transverse (middle) and frontal planes (right) [21] (Copyright Ottobock).

The 7E7 has a mainly titanium construction to reduce its size and weight. Ottobock does not specify a knee prosthesis model or brand to be used with the 7E7 [21]. Instead, the joint can be used with any off-the-shelf knee component.

2.2.4 Ottobock 7E9 hydraulic hip joint

The Ottobock 7E9 is a monocentric hydraulic hip joint that uses a hydraulic damping piston for control (Figure 2.5). The 7E9 provides up to 130 degrees of hip flexion and is recommended for outdoor walking. The 7E9 has a standard male pyramid adapter on the bottom, for use with any off-the-shelf knee joint. Ottobock recommends Ottobock brand knees with the device, such as the 3R60 and 3R106 mechanical knee joints and the C-Leg and Genium MPC knee joints [22].

Figure 2.5 Ottobock 7E9 hydraulic hip joint [22] (Copyright Ottobock).

2.2.5 Ottobock Helix3D and C-Leg

The Ottobock Helix3D hip joint (Figure 2.6) is a commercially available hip joint, introduced in 2008. The Helix3D joint differentiates itself from previous hip prostheses by using a polycentric joint instead of a monocentric design (Figure 2.6 right). The Helix3D four-bar linkage has a varying center of rotation that changes as a function of hip angle [9]. The four-bar linkage allows flexion and extension as well as small abduction and adduction to align the leg during swing. The device features hydraulic control to provide variable resistance to hip rotation during gait. The mechanical damping control is used to adjust step length by modifying where damping occurs and the intensity of the damping during

swing. The device also includes two flexion assist springs that store energy during hip extension and release energy during swing to enable greater flexion angles during swing [9], [23].

The Helix3D has a male pyramid adapter on the bottom that allows the use of any off-the-shelf knee devices with the hip joint; however, Ottobock only recommends the C-Leg and Genium prosthetic knees [23].

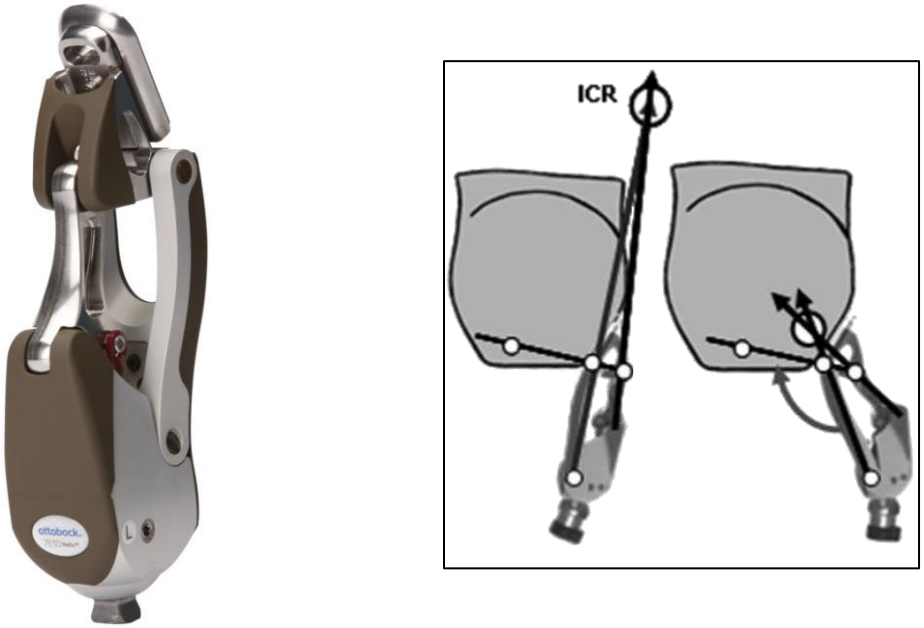

Figure 2.6 Ottobock Helix3D hip joint (left) [24] (Copyright Ottobock) and the polycentric joint's instantaneous center of rotation (ICR) at two different hip angle positions (right, modified from [9]).

2.2.6 Robotic hip-disarticulation prosthesis

Ueyama et al. [12] developed a combined MPC HKAF device that provides DC motor power to both the hip and knee joints. The two DC motors were positioned in the middle of the thigh section and connected to the hip and knee through pulleys. The prosthesis mass without the socket was 9.8 kg. An interesting characteristic was the shared electronic components between the two joints. Both the hip and knee shared a microcontroller, battery, and sensor data, thus reducing the required hardware and enabling hip and knee coordination. The battery was not integrated within the prosthetic leg, and was instead placed into a belt worn around the waist.

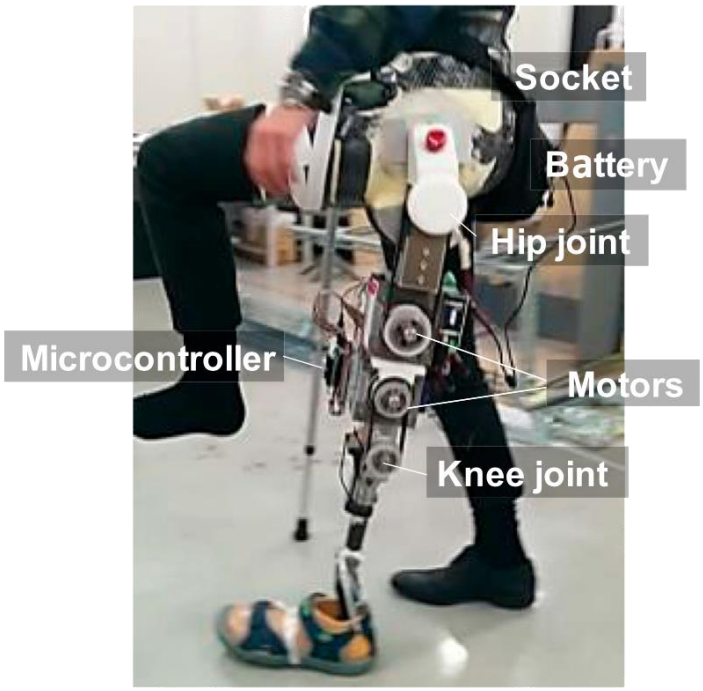

Figure 2.7 Research hip-knee-ankle-foot prosthesis by Ueyama et al. (modified from [12]).

2.3 Synergistic joint control

The Blatchford Linx is the only commercially available MPC prosthesis that integrates the design and control of multiple joints into a single unit. Linx provides transfemoral amputees with hydraulically controlled knee and ankle joints that act synergistically to coordinate walking, standing, slope and stair descent, stand-to-sit, and stumble recovery [25]. Linx uses sensor data to determine the optimal gait mode for the user's environment, and then adjusts knee and ankle resistance profiles to apply different hydraulic resistances at different stages of the gait cycle [26].

Studies are needed to investigate the Linx system in its default walking mode; however, one study [26], [27] investigated Linx behaviour and kinematics when operating in slope descent mode. Participants descended an instrumented ramp with a slope of 5 degrees using Linx with microprocessor control enabled for hydraulically controlled movement, and microprocessor control disabled with joint resistances set to a constant value.

Figure 2.8 Blatchford Linx knee-ankle-foot MPC prosthesis [25].

2.4 Non-amputee and amputee gait

2.4.1 Level walking

Gait characteristics depend on differences between individuals such as sex, weight, height, age, as well as differences in environment (uneven ground, slopes, inclines) [28].

The walking gait cycle consists of stance and swing phases (Figure 2.9). Stance phase is characterized by the leg that is being observed touching the ground, starting with foot contact, progresses through to the mid-stance and late-stance sub-phases until foot-off. Swing phase is when the leg is not in contact with the ground, starting when the foot leaves the ground and swings forward, the leg extends, and then prepares for foot contact. Cycling between stance and swing produces gait, propelling the body forward to provide locomotion. Under healthy walking, stance phase accounts for 60% of the gait cycle. Double support is the period where both feet are on the ground [28], [29].

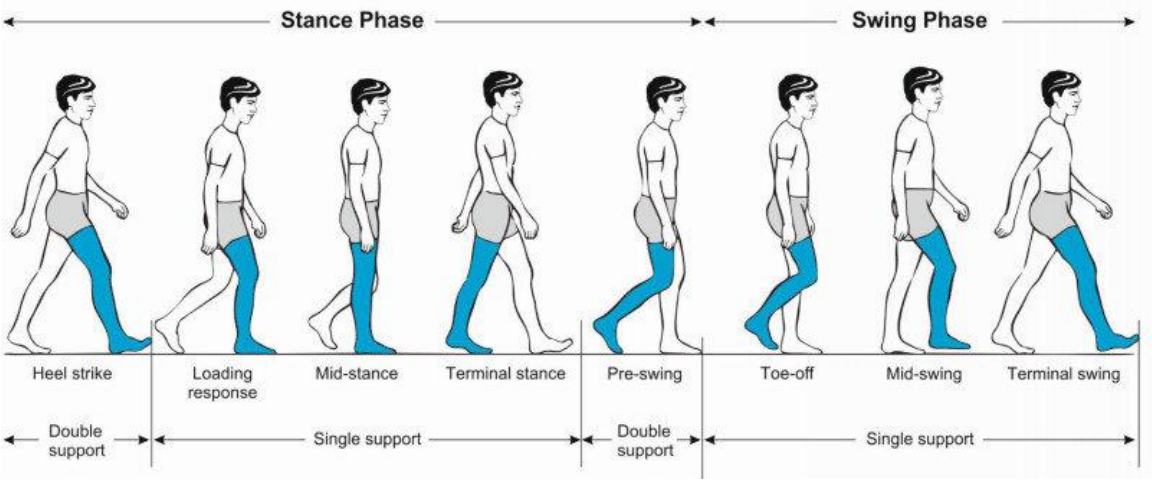

Figure 2.9 Gait cycle phases [30].

During healthy gait, several actions are performed by the body: generation of mechanical energy to maintain or change movement velocity, absorption of mechanical energy for shock absorption, stability, body support during stance, maintenance of upright posture, and control of foot trajectory for ground clearance and foot contact [28].

2.4.2 Hip-level amputee walking

The goal of a prosthesis is to allow amputees to regain their mobility and enable walking. A study by Karimi et al. [31] compared gait characteristics of the sound and amputated limbs of a hemipelvectomy amputee using an Ottobock 7E7 hip with a 3R21 knee joint. The results showed significant gait asymmetry between the intact and prosthetic limbs, where intact hip ROM was 40.30° and prosthetic hip ROM was 27.33°. Intact knee ROM was 46.95° compared to 24.98° for the prosthetic knee. These differences were attributed to hip and knee alignment since, for safety reasons, the knee was aligned just behind the person's load line to induce a knee extension moment during stance. This resulted in the knee remaining in extension for longer periods of stance compared to the intact knee. The study also showed asymmetric pelvic motion and significantly different loads being transferred through each leg, which was attributed to the lack of muscle forces in the prosthetic leg.

Similar gait asymmetry was shown by Schnall et al. [32] when using a mechanical hip joint and MPC knee. Intact leg stance phase was 72% of stride while prosthetic leg stance was about 57%, compared to 60% of stride for able-bodied walking. When compared with able-bodied gait, trunk anterior-posterior lean was greater than normal,

trunk lateral flexion significantly shifted towards the intact limb, and pelvic anterior-posterior motion was greater during early swing.

Similar findings were also reported by Ludwigs et al. [9], with 21 degrees greater range of pelvic tilt compared to an able-bodied control (Figure 2.10). This increased pelvic tilt was attributed to excessively swinging the hips to increase hip flexion during gait. When comparing the Helix3D and 7E7 joints, with both using a C-Leg knee joint, the Helix3D provided more controlled hip motion, where the hip began extending slower than the 7E7 and began flexing before the 7E7 (Figure 2.11a). The Helix3D also provided more controlled hip velocity, which was attributed to hydraulic resistance (Figure 2.11b). Additionally, the Helix3D reached maximum extension at a similar stage in the gait cycle as able-bodied gait, unlike the 7E7 that reached maximum extension very early in the gait cycle (Figure 2.11a).

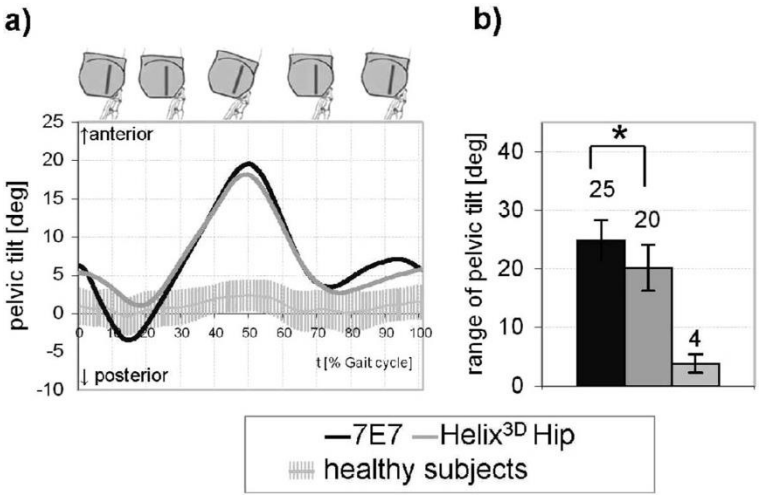

Figure 2.10 Comparison of pelvic tilt patterns (a) and pelvic tilt range (b) between the Ottobock 7E7 hip, Helix3D hip, and an able-bodied control (modified from [9]).

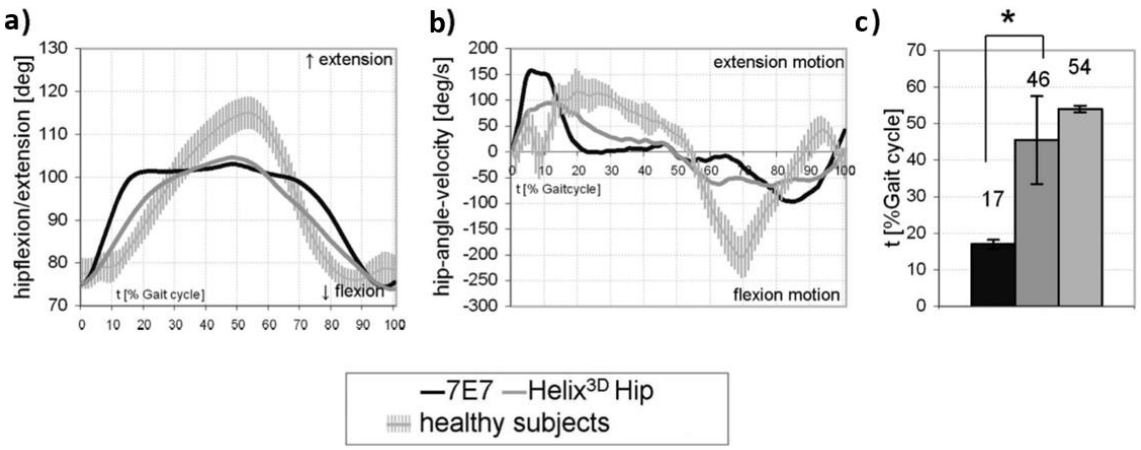

Figure 2.11 Comparison of hip motion (a) and velocity (b) in the sagittal plane, as well as the time of peak extension (s) between the Ottobock 7E7 hip, Helix3D hip, and an able-bodied control (modified from [9]).

Ueyama et al. [12] showed that it is possible to closely mimic able-bodied hip and knee gait patterns when using DC motors to actuate the hip and knee joints (Figure 2.12).

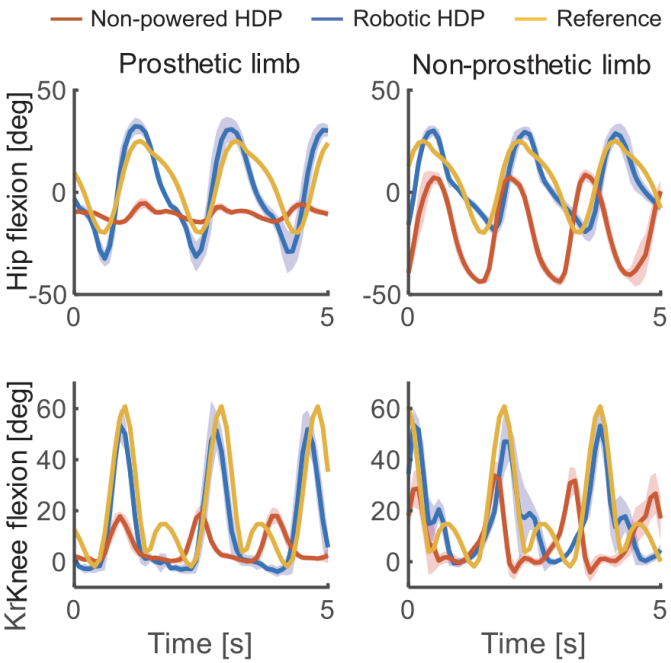

Figure 2.12 Comparison between combined DC motor powered hip-knee prosthesis, Ottobock 7E4 hip and 3R45 mechanical knee, and a control reference [12].

2.5 Summary of literature review

Hip disarticulation amputees require prosthetic hip, knee, ankle, and foot components to enable gait. Typical prostheses separate the hip and knee joints into individual devices and require the prosthetist to combine the available options. This design methodology has benefits that include allowing the prosthetist to choose the best hip and knee combination for their patient; however, combining the hip and knee joints into one unit may provide a more efficient option when providing a MPC controlled hip and knee.

MPC prostheses present many benefits to the user, reducing excessive pelvic motion [9], [32], improving hip joint motion, and improving flexion/extension timing [9]. A typical product would have individual batteries, electronics, and sensors for the hip and knee. In comparison, the research device by Ueyama et al. [12] (Section 2.2.6) showed that it is possible to integrate the hip and knee joints such that they share processing and battery power, which is more efficient than each joint being an independent system. Integrating the two joints also allows for more advanced joint control strategies since sensor data is shared (i.e., processed by a shared microprocessor), possibly allowing better joint

coordination during gait, sit-to-stand, and daily activities. A disadvantage of the Ueyama et al. [12] design is the excessive weight, with a device mass of 9.8 kg.

Integrating the hip and knee joints into a single MPC system can provide benefits for gait control and device efficiency. This integrated component would enable a prosthesis to determine the gait cycle stage or instance and thereby provide optimal joint control for both hip and knee. Additionally, the active hip joint can apply torque to imitate natural gait [12] and reduce excessive pelvic tilt since the pelvis would no longer need to rotate the limb during swing.

Chapter 3: Design and Development

3.1 Design criteria

The design criteria were for a prosthetic thigh unit that included an integrated powered hip joint and MPC dampened knee joint. This Integrated Hip Knee (IHK) unit must be adjustable for a range of thigh lengths. The following sections provide detailed design criteria.

3.1.1 Structural design criteria

Structural design criteria define the shape and size of the design. A set of six structural design criteria were defined:

- The thigh unit must accommodate people with different thigh lengths. Anthropometric data shows that, in the United States, the 5th percentile of upper leg length for females is 31.9 cm [33]. Discussions with a prosthetist determined that the IHK thigh length can be increased by about 10 cm past anthropometric data because the hip joint would be mounted in front of the socket. The minimum thigh unit length should be 42 cm.
- The Össur Rheo knee 3 will be used as the MPC knee joint. This MPC knee automatically adapts with real-time stance and swing control, allows swing initiation on all surfaces, and provides automatic stumble recovery, and manual extension lock. Rheo has an integrated torsion spring that provides an extension bias, and uses magnetorheological fluid to provide controlled rotational damping. The Össur Rheo knee 3 will be integrated directly into the thigh unit structure.
- The chassis will be modular to allow simple modifications to accommodate different hip and knee joints. The device must be able to connect and integrate with different hip prosthesis designs.
- Prosthesis weight must be minimized to reduce the likelihood of prosthesis rejection [3]. The total IHK mass should be similar to the combined weight of the Össur Power Knee (3.2 kg) [34] and Össur Rheo Knee 3 (1.6 kg) [35] (i.e., 4.8 kg).

- The IHK cross-sectional area should be as small as possible to ensure that pants and other clothing can be worn over the device loosely, while still allowing all required electronics to fit within the structure.
- The prosthesis must withstand typical loads during walking without failing. The design will be tested in accordance with ISO-10328:2016 standards, which provide structural tests for lower limb prostheses.
- Loads applied to the prosthesis structure should not transfer to the electronics and other fragile components.

3.1.2 Electronic design criteria

Three electronic design criteria were defined:

- The hip and knee joints must be electronically integrated such that sensor data, battery power, and processing power are shared between the two joints.
- The electronics and battery must power and control the Össur Rheo knee and a DC motor for the hip joint.
- The structure must be instrumented to provide load data to the control system.

3.2 Thigh unit design

The IHK unit has four components (Figure 3.1):

- **Powered hip joint**: The proximal part of the thigh unit is the powered hip joint that is positioned anteriorly to the pelvis and is actuated by a DC motor. The thigh unit is designed to accept different powered hip joint devices. The hip joint used in this research has a male pyramid adapter on its distal end, which is used to connect to the adjustable interface.
- **Adjustable interface**: The adjustable interface is constructed of industry standard prosthetic interfacing components such as male and female pyramid adapters and pylons to allow length and angular adjustment between the chassis and the powered hip joint. The adjustable interface connects to the powered hip joint's pyramid adapter using a female pyramid adapter. The distal end of the adjustable interface can use male or female pyramid adapters or a pylon clamp, depending on the needs of the patient and the decision of the prosthetist.

- **Chassis**: The main structural component of the design. Contains and protects electronics, sensors, and battery used to power and control the Rheo Knee 3 actuator and the powered hip joint. A standard male pyramid adapter can be connected on the top to interface with the powered hip joint.
- **Rheo Knee**: The distal part of the IHK unit is the Rheo Knee 3 actuator oriented upside down so that the proximal surface can screw into the designed aluminum chassis and the male pyramid adapter can interface with the shank components.

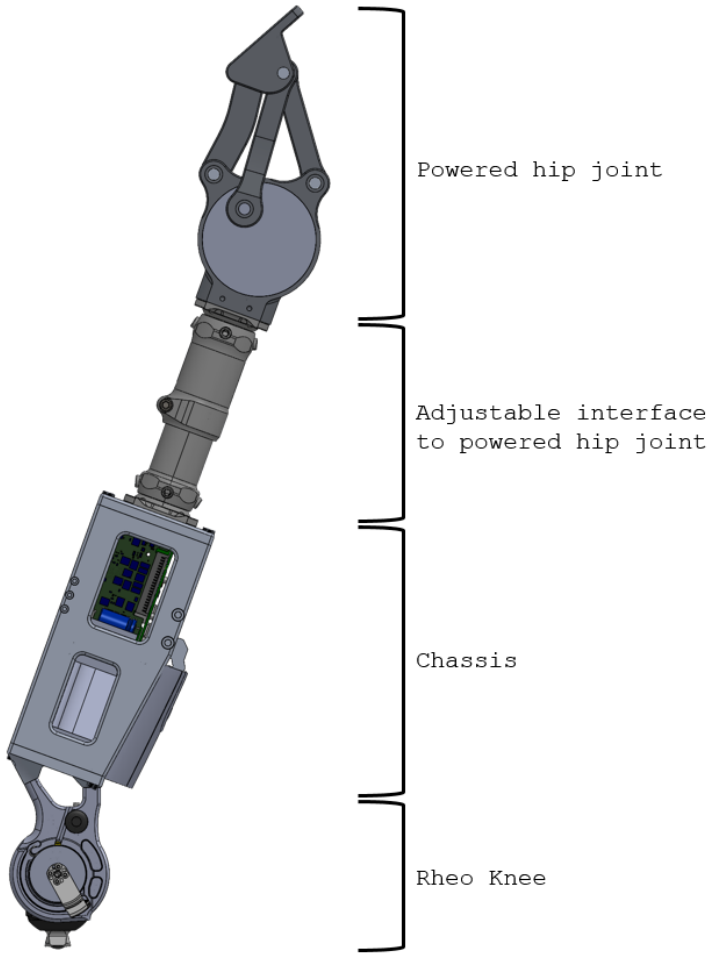

Figure 3.1 Assembled IHK unit consisting of a powered hip, chassis, an interface to connect the powered hip to the chassis, and a Rheo Knee 3 actuator. The interface includes two male pyramid adapters and an Össur height adjustable pylon.

3.3 Electronics and powered hip joint design

The scope of this thesis covers the structural design and testing of the chassis and Rheo Knee 3 integration to create an intelligent thigh unit for a HKAF prosthesis. The design of the powered hip joint, electronics, sensors, and shank components are all designed and unit tested by other members in the project team and will not be discussed in detail in this thesis.

3.4 Design iteration and simulation preparation

A simulation-driven iterative design process was used to develop the IHK chassis component (Figure 3.2). Initial chassis iterations focused on addressing the size-constraining criteria, which included the Rheo Knee connection and the internal volume to

fit the battery and electronics. Afterwards, simulations were used to determine the structural weak points. The chassis design was iterated to improve structural rigidity. Final iterations optimized chassis weight and manufacturability while continuing to use simulations to ensure the design would continue to meet the safety criteria.

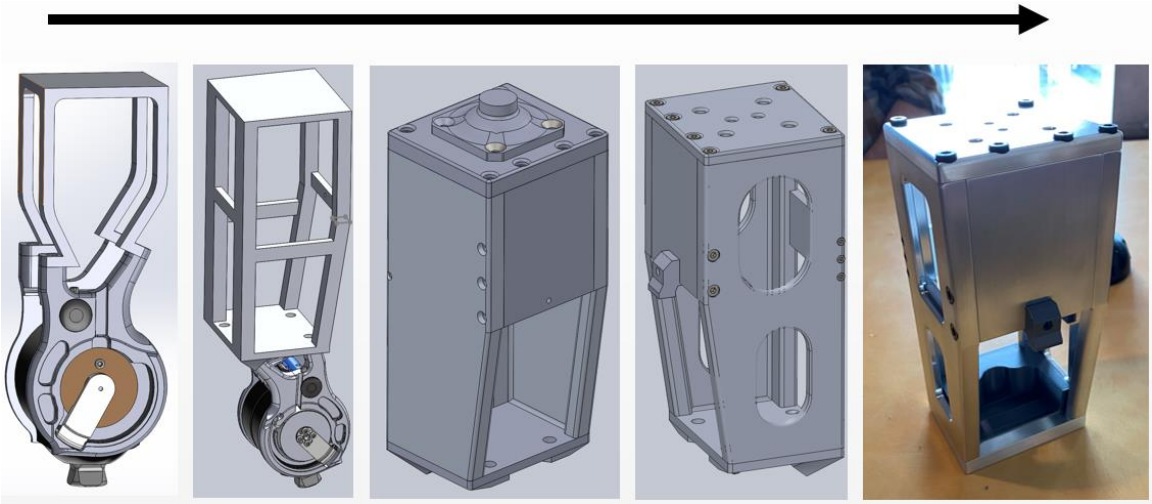

Figure 3.2 Iterations of the chassis. Early iterations focused on addressing size-constraining criteria. Afterwards, iterations focused on testing chassis rigidity and bolt locations. Final chassis iterations focused on weight optimization and ease of manufacturing.

3.4.1 ISO 10328 test criteria

Prostheses undergo a wide range of loading levels and conditions while operating in different environmental conditions. ISO-10328:2016 [36] provides structural testing protocols that include static and cyclic loading tests for foot, ankle, and knee prostheses. The static loading tests simulate peak loads on the prosthesis, while the cyclic tests simulate normal walking activities where loading occurs at regular intervals.

From Table 15 of ISO-10328:2016 [36], the thigh unit is in the category “Complete structure of transfemoral/knee-disarticulation prosthesis or distal part of hip-disarticulation prosthesis without foot unit”. Four required tests in this category include principal structural tests, tests in torsion, test in maximum knee flexion, and tests on knee locks. The tests in maximum knee flexion and the tests on knee locks were considered to be for the knee actuator rather than the device chassis structure. Since the proposed design uses the thoroughly tested Össur Rheo Knee, only the principal structural tests and tests in torsion were considered.

The principal structural tests include a proof load test, an ultimate static load test, and a cyclic fatigue test. Each principal structural test must be conducted under two conditions that simulate the most extreme loads during gait (Figure 3.3) [37]. Loading condition I (LCI) simulates heel strike and loading condition II (LCII) simulates toe-off.

Additionally, different loading levels are defined in ISO-10328:2016. These loading levels simulate variations in individual physical parameters and locomotion characteristics [36], and are referred to as P3, P4, and P5. To simplify simulations and reduce simulation time, only P5 load levels, which have the highest magnitude loads, were simulated. P5 static testing loads are in Table A.1 and cyclic testing loads are in Table A.2.

Reproduced ISO content was copied by Yousef Bader with the permission of the Standards Council of Canada (SCC) on behalf of ISO. The standard can be purchased from the national ISO member in your country or the ISO Store. Copyright remains with ISO.

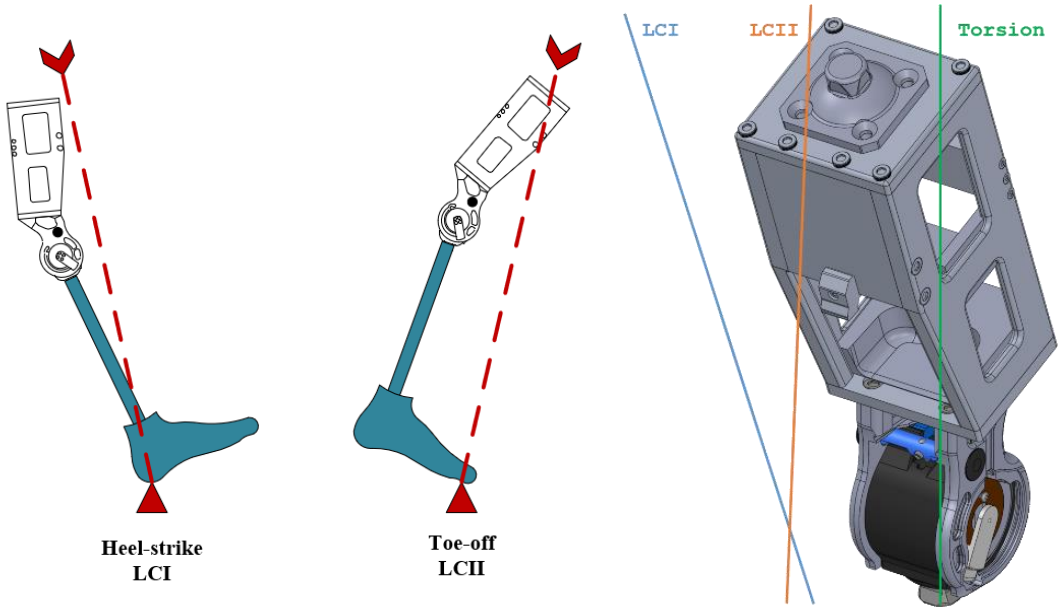

Figure 3.3: Loading conditions as defined by ISO-10328:2016. In the right most image, the blue line represents the LCI loading line, the orange line represents the LCII loading line, and the green line represents the torsion test load axis.

3.4.2 Test rig parts

Three components were designed to replace the Rheo actuator in simulations. Each component allowed loads to be applied along the ISO-10328:2016 [36] loading axes to simplify simulation setup (Figure 3.4**Error! Reference source not found.**). Each test rig

part had the same mounting holes as the Rheo actuator. The test parts were designed to be simple to manufacture and made of aluminum 6061 alloy to ensure ease of material procurement. No simulated load testing was conducted on the Rheo Knee since ISO testing was already completed by Össur.

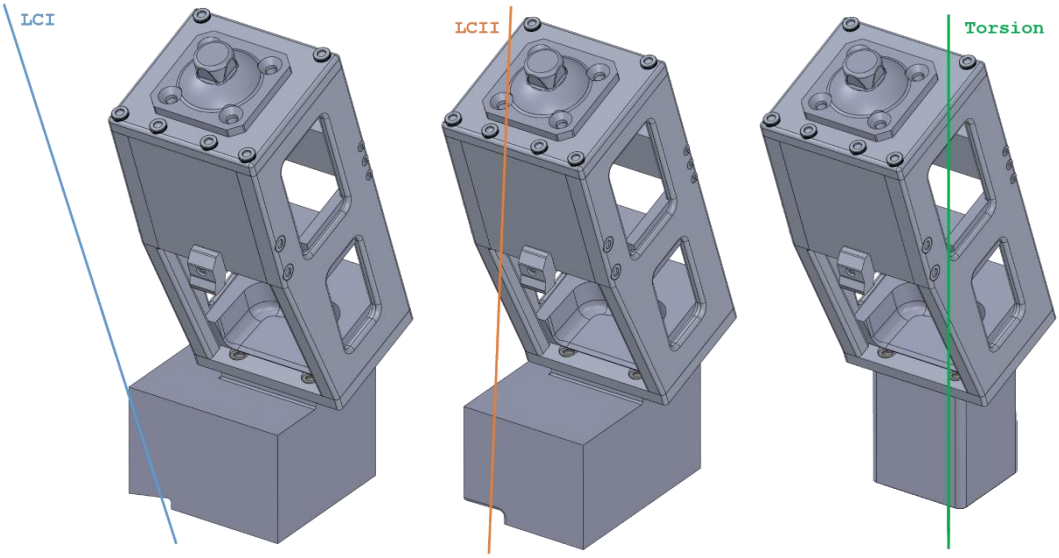

Figure 3.4: Test rig parts for LCI, LCII, and torsion tests used to simplify ISO-10328 simulations. The blue line represents the LCI loading line, the orange line represents the LCII loading line, and the green line represents the torsion test load axis.

3.5 Chassis design

Six aluminum parts are assembled using steel bolts to create the electronics housing structure. Aluminum 2024 alloy was chosen as the chassis material to balance mass, ease of manufacturing, and strength. Three plastic parts were designed to hold a battery in the lower half of the structural chassis, leaving the top half of the chassis to house the electronics that drive hip and knee actuators. Four protrusions from the bottom plate align with the Rheo Knee mounting points, securing the knee actuator to the bottom of the chassis.

Since the hip joint could be mounted in front of the pelvis, the thigh unit must be adjustable to position the knee underneath the pelvis. After consulting a prosthetist, the actuator mounting points on the bottom plate were designed such that the knee actuator is mounted at a 20-degree angle relative to the vertical axis of the aluminum knee structure. This allows the knee actuator to operate at an upright/vertical orientation underneath the pelvis, similar to its orientation in the Rheo Knee, while the rest of the knee structure is

angled 20 degrees anterior to the pelvis. A substitute bottom plate with an angle of 15 degrees was also designed as a precaution if 20 degrees was discovered to be too much during user testing. Further angle adjustments can be made using the pyramid adapters in the interfacing components between the chassis and the powered hip joint, as well as the male pyramid adapter on the Rheo Knee actuator.

3.5.1 Chassis components

Figure 3.5 is an exploded view of the chassis design that accepts a Rheo Knee 3 actuator.

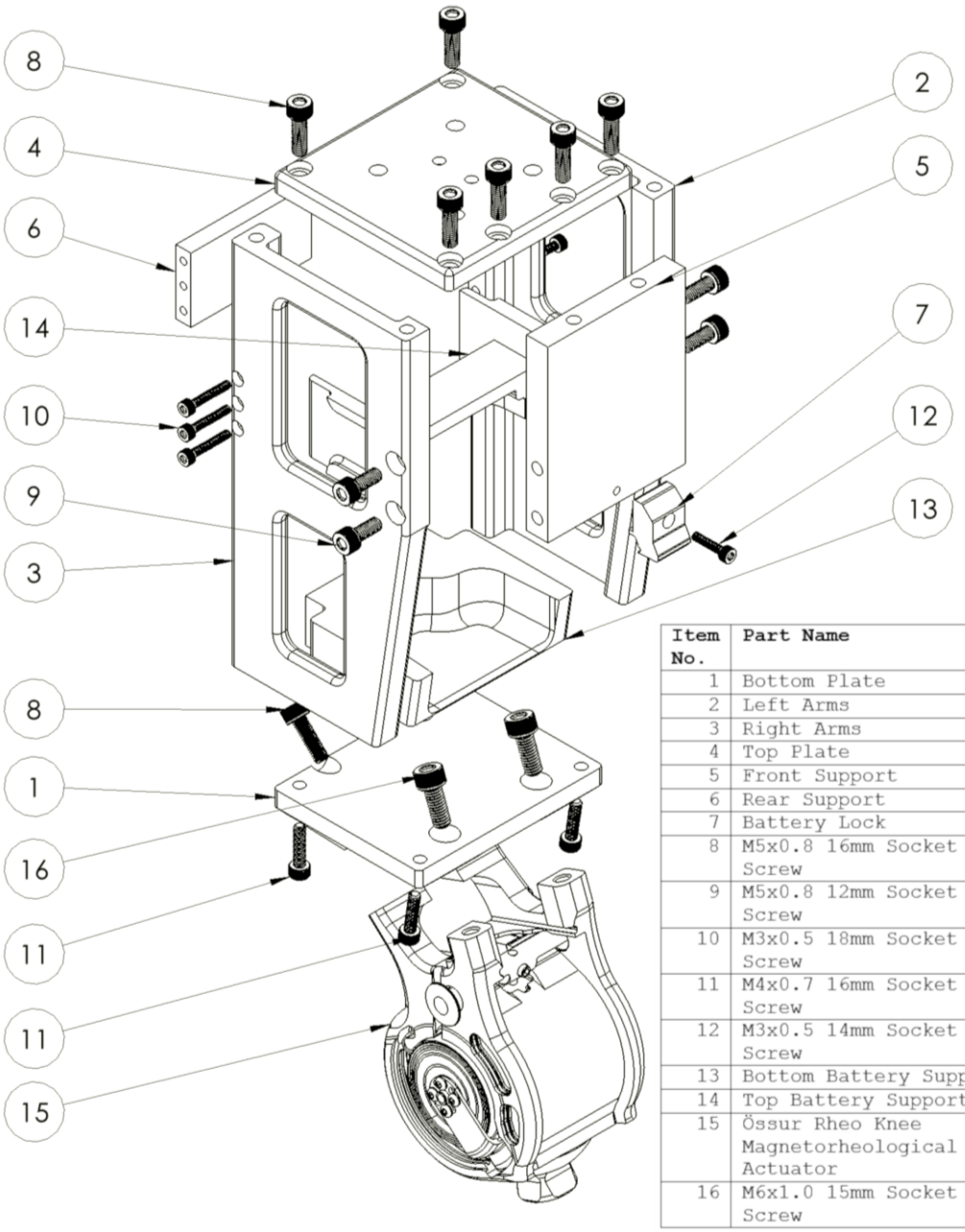

Item No.	Part Name	Qty.
1	Bottom Plate	1
2	Left Arms	1
3	Right Arms	1
4	Top Plate	1
5	Front Support	1
6	Rear Support	1
7	Battery Lock	1
8	M5x0.8 16mm Socket Head Screw	8
9	M5x0.8 12mm Socket Head Screw	4
10	M3x0.5 18mm Socket Head Screw	6
11	M4x0.7 16mm Socket Head Screw	4
12	M3x0.5 14mm Socket Head Screw	1
13	Bottom Battery Support	1
14	Top Battery Support	1
15	Össur Rheo Knee Magnetorheological Actuator	1
16	M6x1.0 15mm Socket Head Screw	2

Figure 3.5 Chassis design and bill of materials.

The left and right side plates were designed to provide the majority of the chassis structural rigidity. The side plates connect all other components together and protect the electronics housed within the chassis. The bottom half of the side plates are sloped to follow the battery geometry. Two holes are cut out from each side plate to reduce device weight and to provide access for positioning and troubleshooting issues with the electronics inside the chassis.

Two 3D printed plastic components tightly hold the battery in the bottom half of the chassis. The bottom battery support sits on the bottom plate and was designed to follow the contours of the side plates to stay correctly positioned. The top battery support is held in place using the cut outs in both side plates. The two battery supports hold the battery in the correct position to connect to the electronics in the chassis' top half, and also position the battery correctly for the 3D printed plastic battery lock to engage the battery tab to keep the battery in the device.

The front and back supports provide torsion resistance to stop the chassis from excessively twisting if subjected to torsion loads. The supports also reinforce the side plates and reduce the amount of bowing the side plates experience under load.

The frontal support also has the additional role of reinforcing the top plate, since the top plate experiences a large bending moment under load. The top plate was designed to accept an industry standard male pyramid adapter to allow prosthetists to connect any hip prosthesis to the structure. The use of a pyramid adapter also allows prosthetists to adjust the hip-knee prosthesis for each user by adding a pylon (i.e., tube to adjust thigh length) and adapters (i.e., angle adjustments). The distance between the knee actuator's center of rotation to the plate's top surface measures 25.1 cm, leaving approximately 16.9 cm to fit a hip prosthesis and connecting hardware to meet the structural design criteria.

3.6 Simulation output analysis

3.6.1 Chassis components

Simulations were prepared and conducted using SolidWorks 2021 Static Studies for ultimate, proof, and torsion tests and Constant Amplitude Fatigue Studies for cyclic tests. The pyramid adapter's domed surface, attached to the chassis top plate, was fixed while the test load was applied to the corresponding test rig part for each test loading condition. All chassis parts were assigned the Aluminum 2024-T4 default material profile available in SolidWorks, and the test rig parts were assigned the Aluminum 6061-T4 default material profile.

The chassis was designed to accept an Össur A-233100 male pyramid adapter on the top plate. However, due to the adapter's complex geometry, a simplified version of the adapter was created to improve simulation times. All electronic and plastic components

were excluded from the simulation to reduce simulation complexity and improve simulation time. The pyramid adapter and bolts were assigned the default Alloy Stainless Steel material profile provided by SolidWorks. Pre-load torque for all bolts was 1 N m.

Table 3.1 Load test passing criteria and simulation results [36].

Load Test	**ISO-10328 Passing Criteria**	**Simulation Result**
Proof load test	Test sample sustains static loading with proof test force (2240 N) for 30 seconds. Maximum of 5 mm of permanent deflection	No chassis permanent deformation under proof load and a maximum elastic deformation of approximately 3.5 mm
Ultimate static load test	Test sample sustains static loading with ultimate test force (4480 N) without failing	Permanent deformation on side arm bottom edges at interface with the bottom plate; however, aluminum structural chassis components will sustain the load Resultant stresses and shear loads from the ultimate static load test were substantially higher than other tests; therefore, results from these tests should be used for bolt analysis
Torsion test	Test sample sustains applied static torque (50 N m) in both directions for 30 seconds Relative angular movement does not exceed 3 degrees	No chassis permanent deformation. The chassis is symmetric; therefore, results are identical in both directions. SolidWorks does not provide angular displacement
Cyclic test	Test sample sustains static loading with maximum cyclic load (1330 N) Test sample sustains cyclic loading for $3*10^6$ cycles Test sample sustains static loading by the final static test force (after cyclic loading) for 30 seconds	Simulations showed that all chassis parts are expected to sustain $3*10^6$ loading cycles. SolidWorks suggests that most parts can sustain upwards of $1*10^7$ loading cycles. Final static test force was not simulated after cyclic loading

After the simulations were completed, the results of each load test were compared to the ISO-10328:2016 standard passing criteria (Table 3.1**Error! Reference source not found.**). In summary, the simulation results suggested that the aluminum chassis components should not experience yielding or failure when subjected to proof, torsion, and

cyclic loading, and a minimal amount of permanent deformation should be expected if the chassis is subjected to ultimate tensile loading. Deformation is most likely to occur at the bottom front edges of the side plates, where the side plates are in contact with the bottom plate. While the simulations provided a prediction of structural component performance, SolidWorks simulations do not simulate the stresses acting on the connectors/bolts used to hold the individual chassis parts together. Separate analysis must be performed to ensure ISO-10328:2016 compliance.

3.6.2 Bolt Integrity Evaluation

After confirming the chassis component's structural integrity, integrity of the steel bolts and aluminum internal threads used to hold the chassis together were evaluated. During the design process, three failure modes were determined to be of importance for bolt analysis: ultimate tensile failure, shearing, and thread stripping.

Ultimate tensile failure can be analyzed using the simulation results discussed in Section 3.6.1. The ISO-898:2013 standard provides the minimum proof load for metric bolts to claim compliance with the standard (Table B.1). Simulation tensile loads results can be compared to the these minimum proof loads to determine if the bolts will fail [38].

The static ultimate test simulations resulted in the largest tensile load on the bolts, therefore these values were used to assess bolt strength. Simulation results showed that class 12.9 bolts provide a minimum safety factor of 2.5 for all bolt sizes used in the chassis.

The equation used to analyze the shear resistance of metric bolts is provided by European Union standard EN1993-1-8:2005 [39]:

$$F_{V,Rd} = \frac{\alpha_V f_{ub} A}{\gamma_{M2}} \tag{B.1}$$

where A is the tensile stress area of the bolt, α_V is a multiplying factor for different bolt strength classes, f_{ub} is the ultimate tensile strength of the bolt, and γ_{M2} is the partial factor for resistance of cross-sections, which is defined as $\gamma_{M2} = 1.25$ for bolts [40].

Simulations showed that ultimate tensile loading tests resulted in the highest shear loading on the bolts. Shear force analysis showed that all bolts should sustain the applied shear loads with a minimum safety factor of 3 when using class 10.9 or greater bolts.

The third failure mode is internal threads stripping under the static ultimate test tensile loads. While there is a risk of both internal and external threads failing, the proposed design uses standard metric steel bolts and the chassis internal threads are made of aluminum 2024 alloy. The internal aluminum threads will fail before the steel threads; therefore, only internal threads were analyzed.

From FED-STD-H28/2B [41], a formula to calculate the required engagement length of an internal thread can be derived given thread dimensions, thread material yield strength, and the tensile load acting on the bolt (derivation shown in Appendix B):

$$L_e = \frac{F_b}{\sigma_{sy}\pi n d_{min}\left[\frac{1}{2n} + 0.57735(d_{min} - D_{2max})\right]} \tag{B.6}$$

where n is the number of threads per unit length (1/pitch), L_e is the engagement length, d_{min} is the minimum value of the major diameter of the external thread, D_{2max} is the maximum value of the pitch diameter of the internal thread, σ_{sy} is the shear yield strength of the thread material, and F_b is the tensile load acting on the bolt. This equation is designed for calculations on imperial bolts; therefore, all metric values were converted to imperial. Aluminum 2024 shear strength is approximately 284 MPa [42]. After calculating the required engagement length for each bolt based on the loading experienced in preliminary simulations, bolt engagement lengths were adjusted to ensure thread shearing does not occur. Simulations were rerun to ensure changes in hole depths did not adversely alter the structural integrity of chassis parts.

3.7 Chassis adjustability

3.7.1 Standard pyramid adapters and pylons

The chassis must accommodate a wide range of adjustment options to allow compatibility with as many prosthesis users as possible. Two levels of adjustment were developed for the chassis: an adjustable interface to the powered hip joint and customized chassis modifications.

The adjustable interface connects the chassis top plate to the powered hip joint using industry standard prosthetic components such as male and female pyramid adapters and pylons (Figure 3.6). Pyramid adapters are industry standard connectors used to attach

prosthetic components to each other while also providing ±10 degrees of angle adjustability in the sagittal and frontal planes (Figure 3.7). Pylons are metal tubes used to add length between two prosthetic components. Pylons are normally cut by a prosthetist or technician to the appropriate size for the person. Pylon clamps secure prosthetic components to either end of the pylon (e.g., four hole mounting clamps and pylon clamps that interface with male and female pyramid adapters).

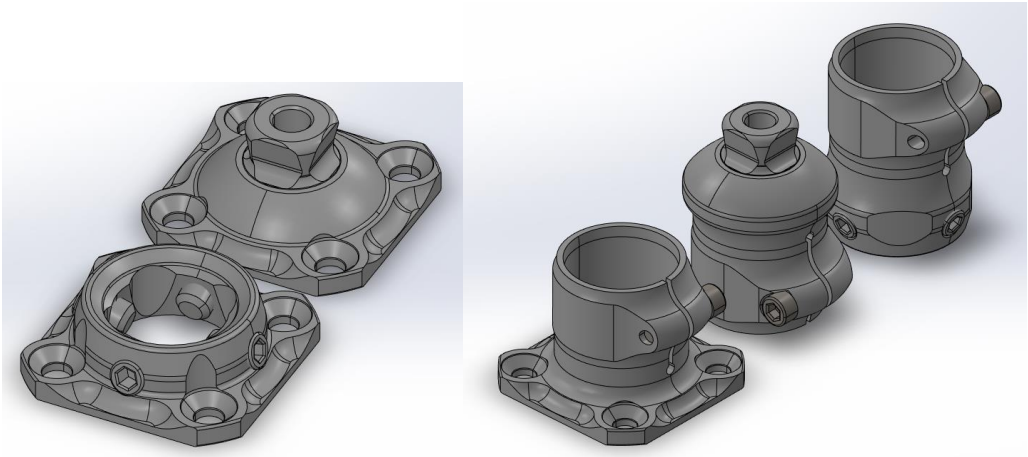

Figure 3.6 Male and female four-hole pyramid adapters (left) and a four hole mount pylon clamp, pylon clamp with a male pyramid adapter, and pylon clamp with a female pyramid adapter (right).

Figure 3.7 Pyramid adapter angle adjustments between the male pyramid adapter of an Össur Proflex XC foot and a pylon with a female pyramid adapter. From the pyramid adapter's neutral upright position (left), the pyramid adapter can provide ±10 degrees of angle adjustment in the sagittal (right) and front planes.

In addition to standard four-hole pyramid adapters, specialized prosthetic adapters can also be used in more unique cases to help prosthetists better adjust prosthesis alignment. For example, double pyramid adapters, offset four-hole pyramid adapters, rotational pyramid adapters, and shift offset pyramid adapters (Figure 3.8). Additionally, pylons can be purchased in adjustable length options, such as the Össur height adjustable pylons [43] that can provide up to 34 mm of length adjustment by sliding the telescopic pylon to the required length (Figure 3.1). By having the option to mix and match different pyramid adapters and pylons, prosthetists would have the ability to adjust the length and align the angles of an IHK to the user requirements.

Figure 3.8 Specialized prosthetic adapters, including a) male-to-male double adapter, b) female-to-female double adapters of different length, c) offset male four-hole adapter, d) offset female four-hole adapter, e) rotation male four-hole adapter, f) rotation female four-hole adapter, and g) adjustable shift female-to-female adapter [44].

3.7.2 IHK range of length adjustments

Using different combinations of adapters discussed in Section 3.7.1, a prosthetist can adjust the IHK length to match the user requirements. The powered hip joint that will be used for IHK testing is 13.9 cm from center of rotation to the most distal point of the joint. The chassis is 25.1 cm from the knee center of rotation to the top surface of the top

plate. To meet the length requirement of 42 cm defined in Section 3.1.1, the adjustable interface must be configurable to a length of 3cm or less. Different configurations of the adjustable interface are detailed in Table 3.2.

Table 3.2 Example adapter configurations and their corresponding interface and IHK lengths.

Components	Interface length (cm)	IHK length (cm)	Comments
Male four-hole pyramid adapter + female four-hole pyramid adapter	2.44	41.44	Shortest possible configuration using only two four-hole adapters. Only provides one pyramid connection for angle adjustment.
Female four-hole pyramid adapter + male-male double pyramid adapter + female four-hole pyramid adapter	4.32	43.32	Shortest configuration that provides two pyramid adapters for double angle adjustment.
Male four-hole pyramid adapter + female-female double pyramid adapter + male four-hole pyramid adapter	4.88, 6.18, 7.68, 9.18	43.88, 45.18, 46.68, 48.18	Provides two pyramid adapters for angle adjustments. Össur manufactures four fixed length female-female double pyramid adapters.
Male four-hole pyramid adapter + pylon clamp with female pyramid adapter + pylon + four-hole pylon adapter	>9.64	>48.64	Provides one pyramid adapter for angle adjustments. Pylons can be made as long as necessary for the patient.
Male four-hole pyramid adapter + pylon clamp with female pyramid adapter + pylon + pylon clamp with female pyramid adapter + Male four-hole pyramid adapter	>11.68	>50.68	Provides two pyramid adapters for angle adjustments. Pylons can be made as long as necessary for the patient.
Male four-hole pyramid adapter + adjustable length pylon with female pyramid adapter ends + Male four-hole pyramid adapter	9.39-11.19, 11.14-14.54	48.39-50.19, 50.14-53.54	Provides two pyramid adapters for angle adjustments. Provides a range of length adjustments without the need for custom length pylons. Össur brand adjustable pylons come in two length options.

3.7.3 Custom chassis components

Customized chassis component adjustments involve manufacturing unique top and bottom plates to accommodate non-standard connections with other prosthetic components. This is enabled by the chassis' segmented design that allows individual parts to be removed and replaced without the need for completely disassembling the chassis. For example, multiple iterations of the chassis bottom plate were manufactured to test different knee joint configurations (Figure 3.9). A modified version of the original bottom plate was

designed and manufactured with a 15-degree knee joint angle to test knee alignment with different angles. A bottom plate was also manufactured that would accept a pyramid adapter, like the top plate, instead of having Rheo knee actuator mounting points.

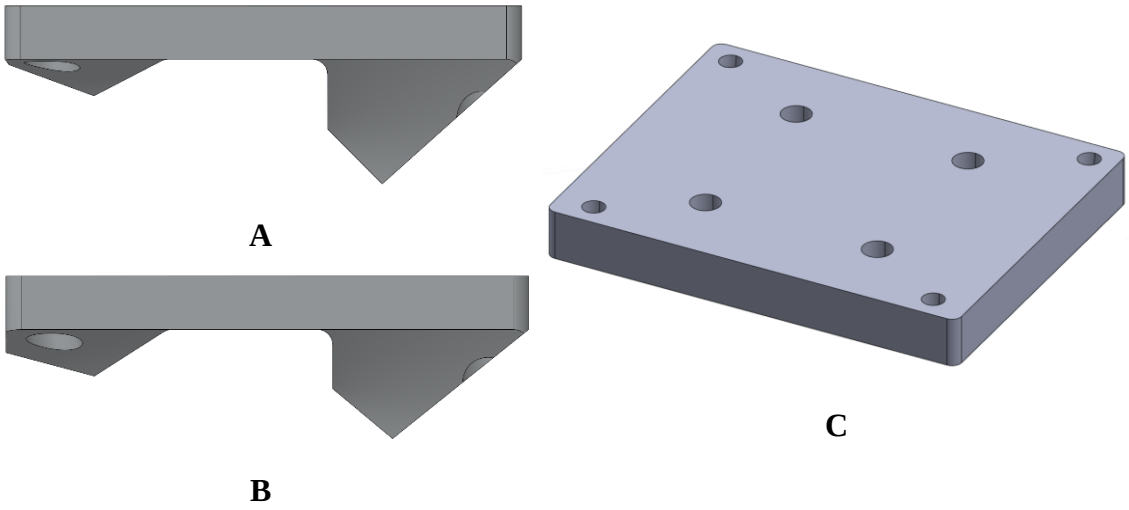

Figure 3.9 20 degree (A) and 15 degree (B) bottom plates, and an alternate bottom plate designed to accept a pyramid adapter (C).

Similarly, top plate versions were also created to interface directly with the motor for some hip designs, instead of using the original adjustable interface (Figure 3.10). Top plate modification helps reduce IHK length by cutting out the pyramid adapter, allowing the chassis to meet length requirements with larger and longer hip joints; however, this configuration loses adjustability between the chassis and the powered hip joint.

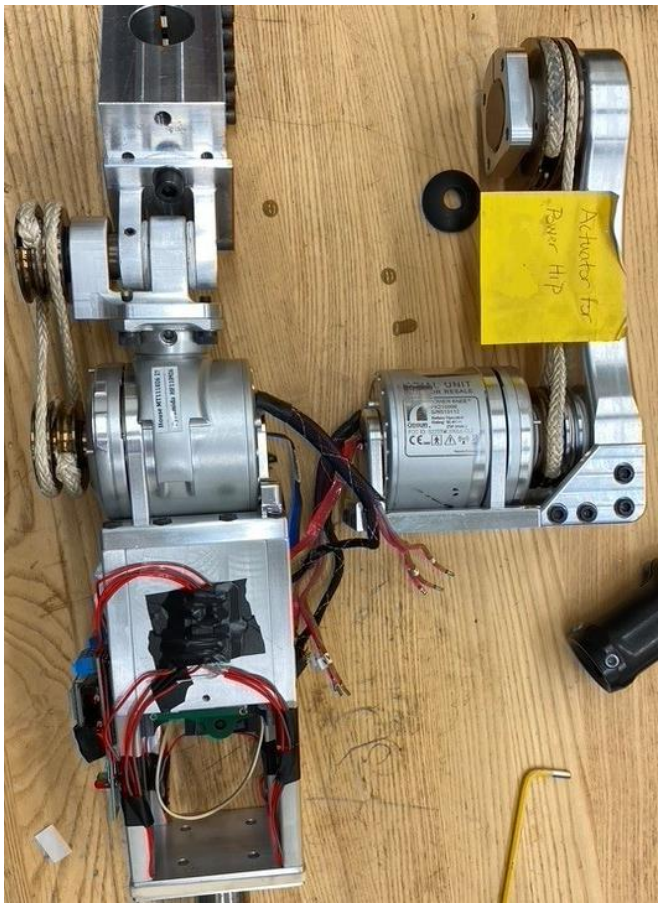

Figure 3.10 Front and lateral mount powered hip joints with customized top plates to directly attach to the chassis, bypassing the need for pyramid adapters.

Chapter 4: Bench Testing

4.1 Chassis testing

After designing and simulating the chassis, the design needs to be physically tested to verify simulation and calculation results and to ensure structural stability for use in a HKAF prosthesis. Structural testing involves mechanically loading the chassis. Since ISO-10328 was used as a guideline for simulations, it was also used for bench testing.

Simulations predicted that ultimate static test loading would result in permanent deformation of the chassis; therefore, only proof load testing was conducted to preserve the structural integrity of the chassis for user testing in a complete IHK unit.

4.1.1 Test tools and preparation

An Instron 4482 machine was used to proof load test the chassis. An adapter plate was designed to attach the chassis to the Instron's top moving arm using the pyramid adapter mounting holes on the top plate. The P5 LCI test rig used for simulations was manufactured to apply the P5 proof load in LCI. A loading rig was manufactured with a long cylindrical structure with a semi-spherical surface at the tip. The loading rig was placed underneath the test rig and secured using T-clamps.

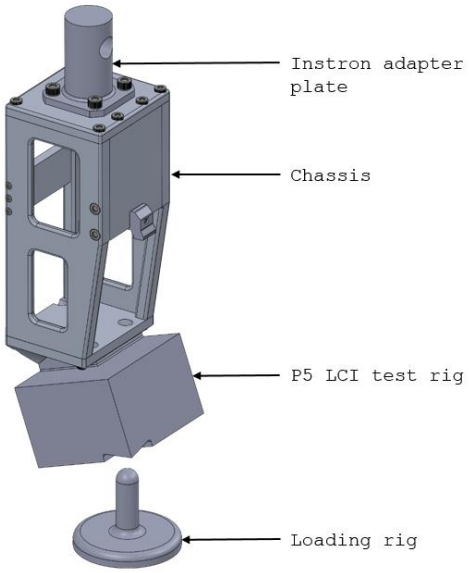

Figure 4.1 Bench testing setup used to structurally test the chassis.

The Instron machine was operated by inputting the required rate of descent, in mm/min, as well as the test end load. When a test started, the Instron machine moved the chassis down and the test rig pushed against the loading rig. The resultant force between the loading rig's spherical surface and the test rig's flat surface was perpendicular to the flat surface, and therefore the resultant force vector acted along the loading line as specified by ISO-10328 [36]. Figure 4.1 shows the testing parts used in the structural testing.

4.1.2 Test procedure

The following steps outline the modified procedure used to structurally test the chassis, as defined by ISO-10328 proof load testing guidelines [36]:

1. Assemble the Instron adapter plate to the top plate and the test rig to the bottom plate of the chassis.
2. Insert the Instron adapter plate into the upper moving arm of the Instron and secure it with a pin.
3. Position the loading rig underneath the test rig such that it aligns with the location of the loading surface of the test rig.
4. Secure the loading rig to the bottom plate of the Instron used T-slot clamps.
5. Lower the chassis slowly until a 1024N settling load is applied. The load is held for more than 10 seconds and less than 30 seconds.
6. Raise the Instron until no force is applied to the chassis. Let the chassis rest for a period of 10-20 minutes before continuing.
7. Program the Instron to move the chassis downwards, loading the chassis at a rate of 100-250N/s until the applied load is in the range of 2200 – 2500N. Maintain the applied load for 30(±3) seconds.
8. Raise the chassis slowly until the applied force is in the range of 50-100N (stabilizing load) and hold for around 5 minutes.
9. Raise the chassis until it is no longer in contact with the loading rig.
10. Save recorded data and analyze the chassis to identify any potential points of failure or permanent deformation.
11. Repeat steps 5-10 as necessary to collect further data.

4.1.3 Results and discussion

After all parts of the chassis were manufactured and assembled, they were then attached to the Instron 4482 machine for testing (Figure 4.2). While programming the Instron machine, some difficulties were encountered that reduced result accuracy and several compromises had to be made.

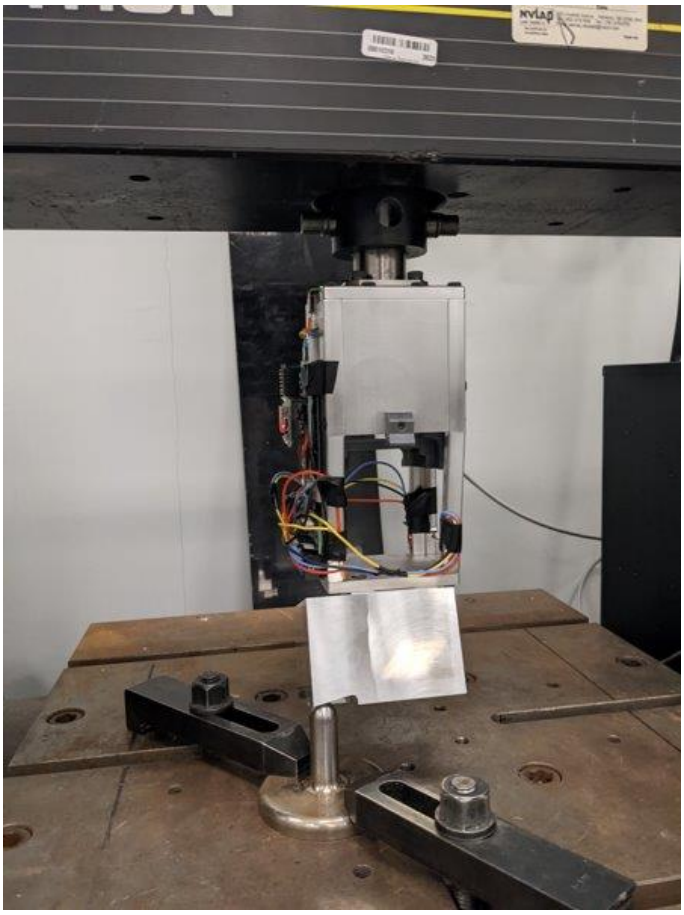

Figure 4.2 Test setup of the chassis using an Instron 4482 test machine. The Instron adapter plate is inserted into the Instron moving arm using a pin.

The first limitation was that the Instron control software does not allow users to program a test procedure that targets a required loading rate. The test procedure detailed in Section 4.1.2 requires the test load to be applied at a rate of 100-250N/s, however the software only allows users to program a rate of descent in terms of distance per unit time. As a compromise, several different descent speeds were tested, and the output load data was analyzed to find settings that provide loading in the required range of values. A descent rate of 5mm/min was found to produce a loading rate of about 125N/s.

The second limitation that was encountered was that the software does not allow users to program complex loading operations, limiting the user to only program test procedures that start at rest, apply a load, and then return to rest. Due to this limitation, it was not possible to correctly apply the stabilizing load after the chassis was tested at proof load. As a compromise, the chassis was fully unloaded to a rest position after proof loading, and then a new test was started to load the chassis to the stabilizing load.

Finally, electrical noise was observed in the Instron force output that resulted in an approximate ±20N variation in load. While the noise is insignificant during proof loading, it made it difficult to correctly apply the stabilizing load.

Although several compromises were required to complete the test procedure, the main goal of the test, which was to verify the simulation results and structural integrity of the chassis, was completed. No permanent deformation or bending was observed on any of the chassis components, and none of the threaded holes appeared to be damaged after testing. By using the Instron displacement measurement readout, it was possible to determine if the chassis had experienced permanent deflection by measuring the displacement at which the chassis came in contact with the loading rig before and after proof load. The chassis did not experience noticeable permanent deflection after proof loading, therefore meeting the passing requirement for proof load testing as defined in Table 3.1**Error! Reference source not found.**.

4.2 Strain gauge testing and calibration

The thigh prosthesis requires sensors to provide an intent recognition algorithm with sufficient data to perform optimally [6]. The Rheo Knee 3 actuator provides knee angle data. Applied loads on the chassis are measured by a set of strain gauges adhered to several locations along the distal end of the side plates of the chassis. The strain gauges and supporting electronics must be tested and calibrated to ensure that quality loading data can be collected and later used by an intent recognition algorithm to provide correct control to the knee and hip actuators.

4.2.1 Test tools and preparation

Strain gauge testing used the same tools as chassis structural testing (section 4.1.1); however, additional preparation for sensor calibration included adhering the strain gauge

sensors to the chassis and preparing a conditioning circuit to collect sensor data as the chassis is tested using the Instron.

Based on simulation analysis, the chassis would experience peak strain on the bottom of the front columns on the left and right sides, above the mating surface with the bottom plate (Figure 4.3). This area on the chassis is convenient for strain gauge application since it is a flat area with sufficient space for cable management; therefore, two strain gauges were placed on each front column in perpendicular configurations.

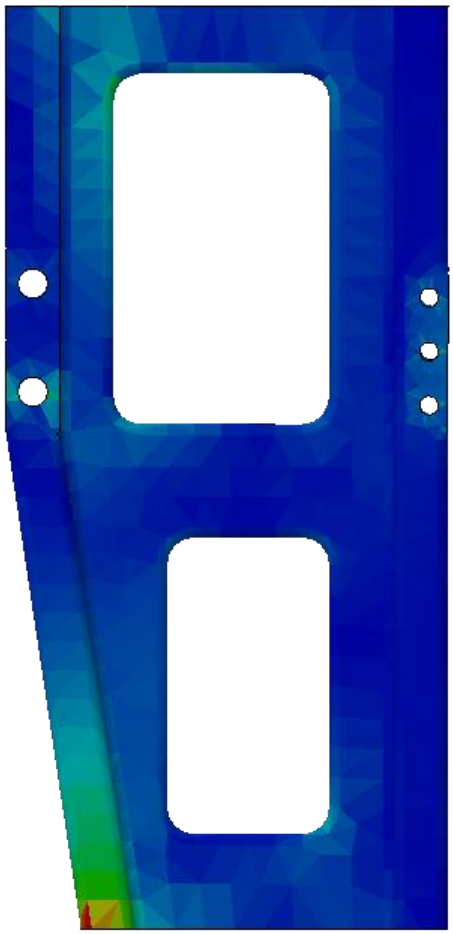

Figure 4.3 Strain simulation results from ultimate tensile load applied in LCI. High strain concentration is observed on the front column of the chassis.

When a load is applied on the chassis, the stress is transmitted throughout the chassis through the four columns; therefore, it was decided to apply and additional four strain gauges onto the rear columns to instrument all four supporting columns of the chassis. Unlike the front columns of the chassis, simulations showed that the rear columns will not experience high concentrations of strain, therefore one of the tasks during the

calibration procedure is to tune the amplifier and software gain values to ensure rear column load values have similar magnitude readings as the front column load values.

By instrumenting all four columns of the chassis, it becomes possible to accurately measure total load applied to the chassis by adding the measured loads from each chassis column. Additionally, since the strain gauges will be placed on each of the four corners of the chassis, it becomes possible to determine the direction of the load vector on the leg. Knowing the direction of applied load allows the intent algorithm to estimate torque acting on the chassis and to determine where load is being applied on the foot, which allows the intent algorithm to determine the user's stage of stance.

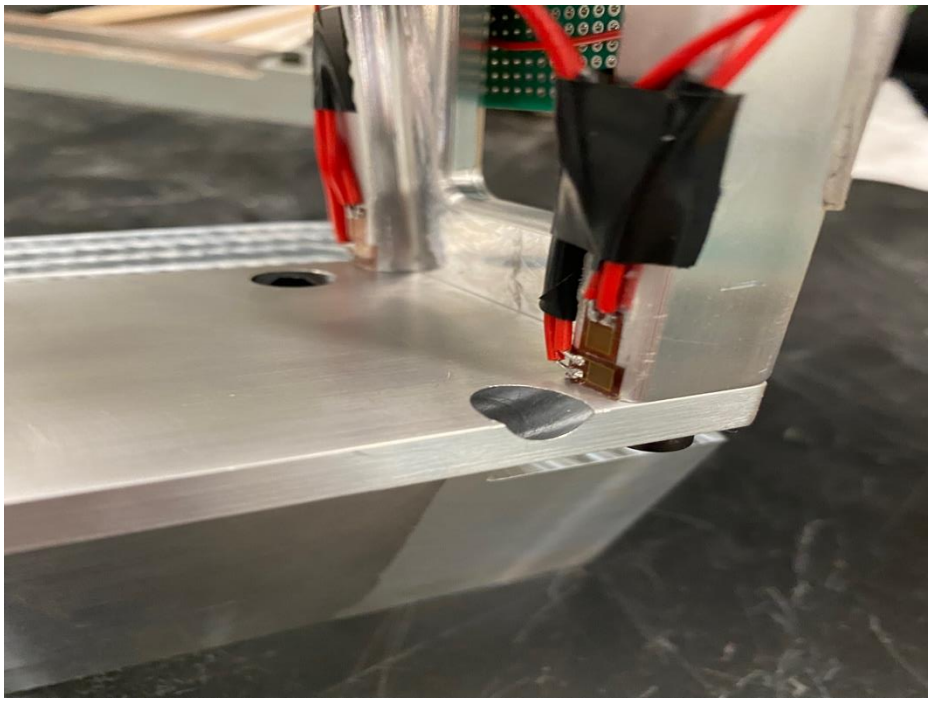

Figure 4.4 Strain gauge pairs adhered in perpendicular orientations at each corner of the chassis for load measurements.

The eight strain gauges were divided into two groups of four gauges: one group adhered to the front two columns of the chassis and the other group is adhered to the rear two columns (Figure 4.4). Each group of strain gauges was then individually wired into a Wheatstone bridge. The outputs of both Wheatstone bridges were connected to an AD7124-8 24-bit analog-to-digital converter (ADC) (Analog Devices). The AD7124-8 also provides programmable signal amplification and digital signal filtering, reducing the required components needed for the conditioning circuit. Outputs from the AD7124-8 were sent to an ESP-32 based microcontroller for further data processing, local data storage to

an SD card, and data transmission via Bluetooth to a laptop for live monitoring of the strain gauge outputs and remote data recording (Figure 4.5).

A more detailed diagram and a bill of materials for the data conditioning and collecting system can be found in Appendix D.

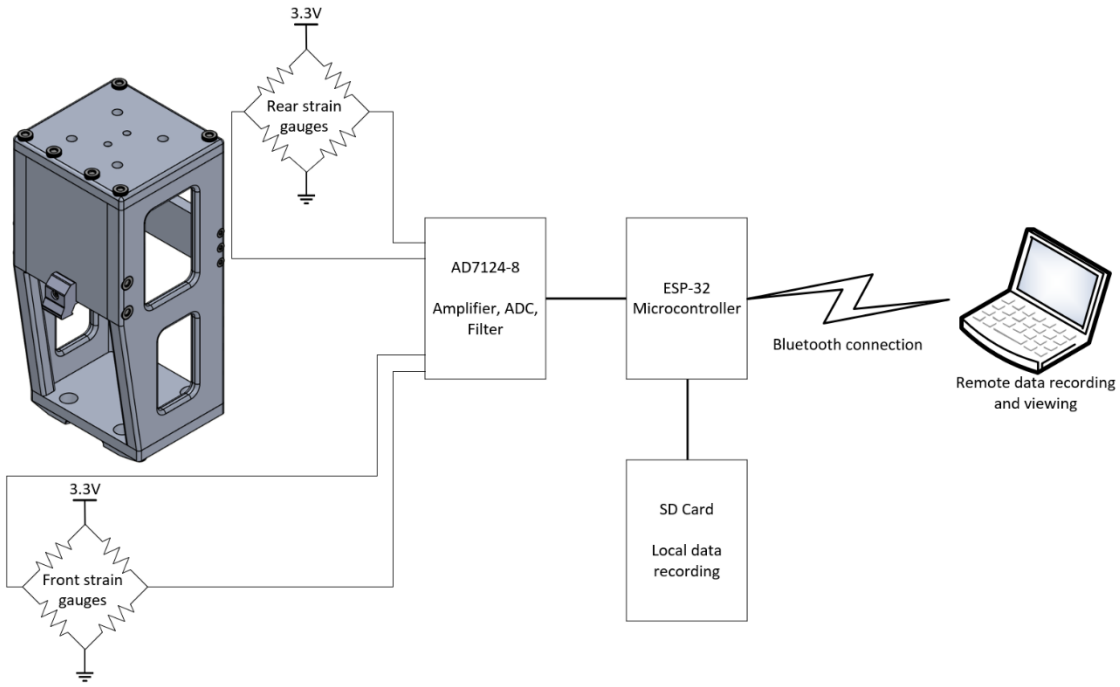

Figure 4.5 Simplified diagram of the electronics system used to calibrate the chassis load sensors during testing. Wheatstone bridges are connected to an AD7124-8 to amplify, digitize, and filter the sensor readings. The processed data is sent to an ESP-32 microcontroller that locally records data to a SD card and sends the data via Bluetooth for remote viewing and recording on a laptop.

4.2.2 Test procedure

1. Assemble the Instron adapter plate and the test rig to the chassis.
2. Insert the Instron adapter plate into the upper moving arm of the Instron machine and secure it with a pin.
3. Position the loading rig underneath the test rig such that it aligns with the location of the loading surface of the test rig.
4. Secure the loading rig to the bottom plate of the Instron machine using T-slot clamps.
5. Move the chassis downwards slowly until a force of 1024N is applied to the chassis. This load should be held for more than 10 seconds and less than 30 seconds.

6. Raise the Instron machine until no force is applied to the chassis. Let the chassis rest under no load until strain gauge outputs settle.
7. Program the Instron machine to lower the chassis slowly to reach a loading rate of about 50N/s until a load of about 2300N is reached.
8. Hold the chassis under load for 10 seconds or until the chassis strain gauge data stabilizes.
9. Raise the chassis until it is no longer in contact with the loading rig.
10. Save the data from the Instron machine and the chassis strain gauges.
11. Repeat steps 5-10 as necessary to collect sufficient data for analysis. Repeat testing with faster loading rates if required.

4.2.3 Observations

A total of 50 tests were conducted to collect data for load sensing testing and calibration. The tests used three programmed Instron speeds (1mm/min, 5mm/min, and 10mm/min) to test the effect of loading rate on the calibration factor of the gauges. Some tests exhibited motion artifacts that affected the quality of the test results. Observed motion artifacts were categorized into three different types:

- Type 1 artifacts are abnormalities that appeared equally in both chassis' sensor and Instron data (Figure 4.6a).
- Type 2 artifacts are abnormalities that appeared in both chassis' sensor and Instron data; however, the abnormality magnitude appears larger in the chassis sensor data (Figure 4.6b).
- Type 3 artifacts are abnormalities that only appeared in the chassis' sensor data (Figure 4.6c).

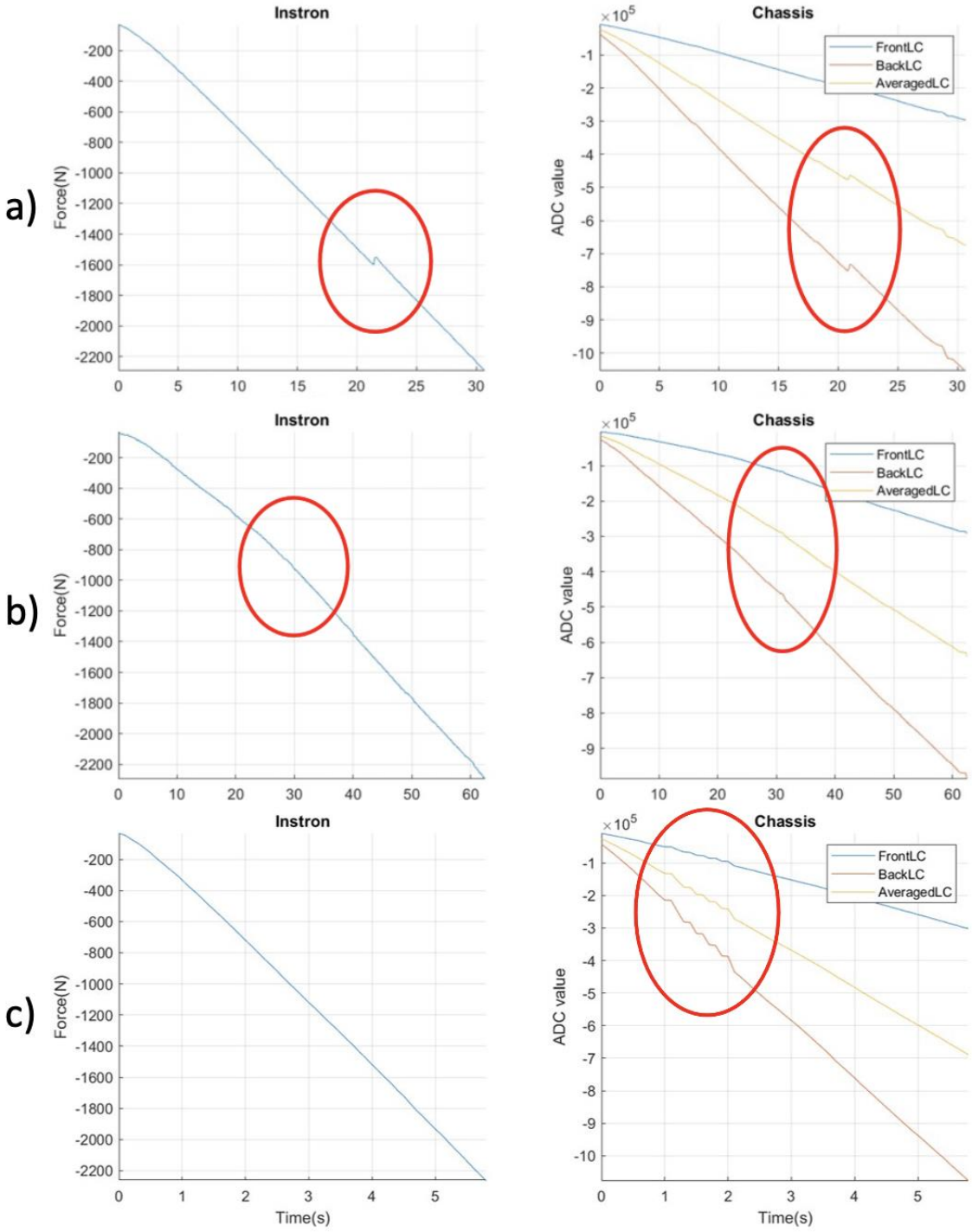

Figure 4.6 The three types of motion artifacts observed during calibration load tests of the chassis sensors. a) Type 1 artifacts appear in chassis sensor and Instron load data with similar relative magnitude. b) Type 2 artifacts appear in both sets of collected data but have a higher relative magnitude in the chassis sensor data. c) Type 3 artifacts only appear in the chassis sensor data.

The artifacts had several potential causes:

- The connection between the Instron adapter plate and Instron moving arm has some play due to loose tolerances between the adapter plate, the sleeve that the adapter plate is seated into on the moving arm of the Instron machine, and the pin that secures the adapter plate in position. As the chassis is pushed downwards against loading rig, sliding occurs resulting in movement of the chassis while loading is applied.
- The chassis sensors and conditioning circuit may be more sensitive to smaller movements of the chassis, thus resulting in recorded motion artifacts appearing at higher magnitudes compared to the Instron data.
- Post-test analysis on the chassis and test rig parts showed that the P5 LCI test rig loading surface had deformed slightly due to repeated contact with the loading rig (Figure 4.7). The motion artifacts may have been caused by the P5 LCI test rig moving against the loading rig as load was applied and getting caught on these deformations.

Table 4.1 summarizes the conducted calibration tests and artifact occurrence. Testing started at slower speeds (1mm/min) before increasing Instron speed. As testing progressed, motion artifacts became more common. This could be the result of the deformation of the P5 LCI test rig progressively worsening as each test was conducted.

After testing was concluded, one of the strain gauge wires broke when handling the chassis, requiring strain gauge replacement due to damage to the solder pad. Considerations were made to ensure more careful handling of the chassis in the future to avoid further damage to the electronics.

Figure 4.7 Observed deformation of the loading surface of the P5 LCI test rig after completing Instron load testing.

Table 4.1 Summary of calibration tests and occurrence of motion artifacts.

Instron speed (mm/min)	**Number of conducted tests**	**Number of tests with observed motion artifacts**
1	27	3
5	13	7
10	10	4

4.2.4 Calibration

Using the collected data from the Instron testing, a calibration methodology was defined and used to convert the strain gauge ADC bit values to the applied load on the chassis. Test samples that showed motion artifacts were excluded from the calibration process. The calibration method is as follows:

1. Add the ADC values from the front and rear strain gauges to obtain overall values for load on the chassis.

2. Curve fit the overall loading values of individual test samples to the collected Instron data.
3. Extract the polynomial coefficients from the fitted curves for each test sample.
4. Average polynomial coefficients across all test samples.
5. Apply the averaged polynomial coefficients on the raw test sample data to determine the root mean square error (RMSE) and correlation values.

The calibration process was repeated to compare the results of 1st, 2nd, and 3rd order polynomial curves and the lowest order curve that would produce acceptable error was chosen. For each polynomial order, RMSE was calculated for each individual test sample and then averaged across all test samples (Table 4.2). Results showed minimal improvement between 2nd and 3rd order polynomial fitting, therefore 2nd order polynomial curve fitting was used to convert the ADC output values to chassis load.

All test samples were tested up to a programmed load of 2300N. Therefore, the calculated RMSE of 31.63N was deemed to be acceptable since it would be unlikely that a relatively small error would affect intent recognition algorithms.

Table 4.2 Root Mean Square Error results for different polynomial fits.

Polynomial curve fit	**Root Mean Square Error average for all included tests (N)**
1st order calibration	35.93
2nd order calibration	31.63
3rd order calibration	31.35

4.3 Bench testing summary

Bench testing performed on the chassis verified results obtained from simulations and confirmed the structural integrity of the proposed IHK unit, while sensor calibration verified that repeatable and accurate sensor measurements could be obtained from strain gauges on the chassis.

Chapter 5: Device Evaluation

Device evaluation on a complete IHK unit was completed using a hip prosthesis simulator that was designed and built by the Power Hip Research team to allow able-bodied people to walk on an HKAF prosthesis [45]. Device evaluation was performed to verify that the mechanical design was able to produce viable walking gait. Joint angle parameters were collected to assess Rheo knee actuator performance and correct hip actuator motion. Videos were recorded to determine gait characteristic parameters. The test protocol was approved by the University of Ottawa Office of Research Ethics and Integrity (Appendix E).

5.1 Testing methodology

5.1.1 Test prosthesis

The test prosthesis consisted of the IHK assembled with a front-mounted powered hip joint attached directly to the top of the chassis using a custom top plate mount. A pylon connected an Össur Pro-Flex XC foot [46] to the IHK to complete the HKAF prosthesis.

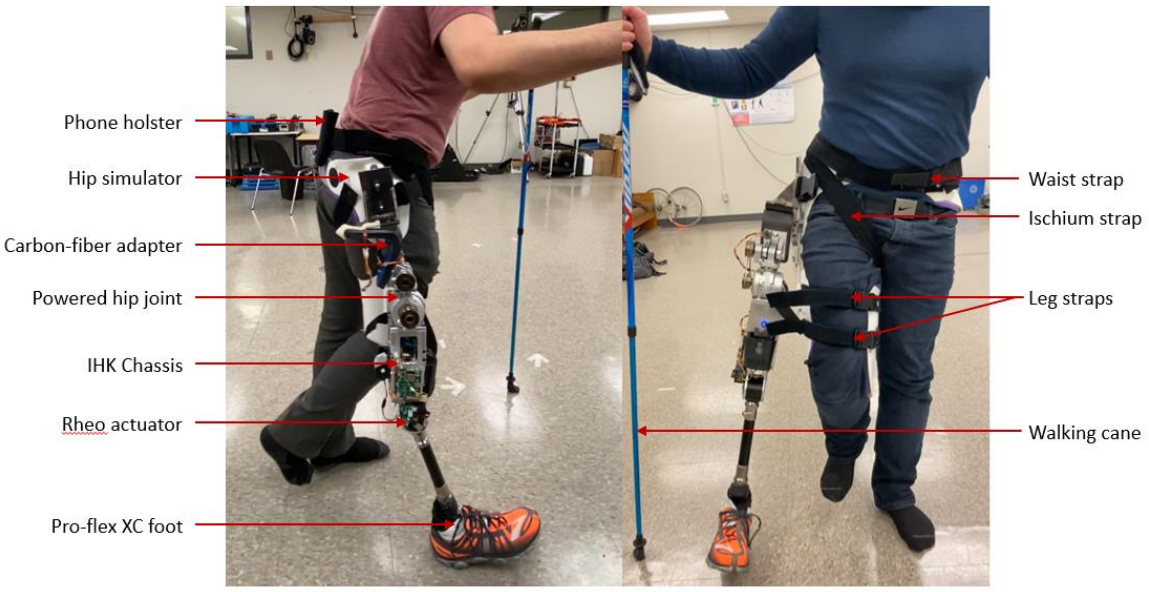

Figure 5.1 Test prosthesis setup attached to hip simulator.

A custom carbon fiber adapter plate wan designed and manufactured to attach the IHK to the simulator. The simulator was secured to the participant using two straps around

the leg, one strap around the waist to tighten the pelvic basket, and one strap underneath the right ischium (Figure 5.1). A phone holster was secured above the simulator to position a smartphone on the pelvis for pelvic data recording.

Mass of the simulator and HKAF, as well as sub-components, are shown in Table 5.1. The combined hip-knee electronics were still in development at the time of testing, therefore separate microprocessors and batteries were included for each joint. As a result, the IHK mass was higher than planned; however, mass can be reduced in future versions through electronics optimization. Several options were available to ensure the prosthetic limb and the contralateral limb were the same length:

- Prosthesis length was adjusted using different pylon lengths.
- Contralateral limb length was adjusted using a shoe that had been modified to increase sole thickness.
- The right ischium strap was used to raise and lower the hip simulator basket to quickly fine tune leg lengths to achieve neutral pelvis alignment.

Table 5.1 Test prosthesis assembly mass, including electronics and batteries.

HKAF Components	Mass (kg)
Hip simulator + HKAF	9.5
HKAF	6.25
IHK	5
Shank + ankle + foot	1.25

5.1.2 Participants

For safety, only able-bodied individuals participated in preliminary test trials with the assembled IHK and the hip simulator. Three male participants volunteered to test IHK functionality (Table 5.2). Each participant had previous walking experience on the hip simulator with the powered hip joint assembled with an Össur Rheo Knee 3 and an Össur Pro-Flex XC foot, as well as an Ottobock Helix3D hip joint assembled with an Össur Rheo Knee 3 and an Össur Pro-Flex XC foot. Participants were given the option of using one or two canes. Participant A had the most experience walking on the hip simulator, and had

trained to walk on the hip simulator for a longer period of time and on more hip prosthesis joints than participants B and C.

Table 5.2 Participant information.

	Participants		
	A	**B**	**C**
Age (years)	44	28	26
Height (cm)	178	180	175
Mass (kg)	95	95	98
# of canes	1	2	2

5.1.3 Control system

At the time of testing, the gait intent recognition algorithm was still in-development. Therefore, the hip joint was programmed to follow a predefined joint position and angular velocity profile that mimics level ground walking (Figure 5.2). After completing tuning and initial testing with the IHK, the hip angle trajectory was programmed to have a 0° maximum extension and 36° maximum flexion for a total range of 36° over 2.5 seconds, resulting in a cadence of 24 steps/min.

The gait profile was uploaded into the hip joint control software, which would attempt to follow the gait profile using its control system to match the requested joint angles and angular velocities. A laptop connected to the IHK through Wi-Fi and Bluetooth connectivity initiated and stopped both data collection and powered hip rotation.

The knee actuator used a mostly unmodified Rheo Knee 3 control system, with the main difference being load inputs from chassis strain gauges instead of typical shank forces (Section 4.2.1). Initial feedback from the participants showed that the knee was not entering swing phase mode and remained locked in extension throughout swing phase; therefore, minor changes were made to the control system to make the stance detection functionality less sensitive and allow the knee to enter swing phase and flex properly.

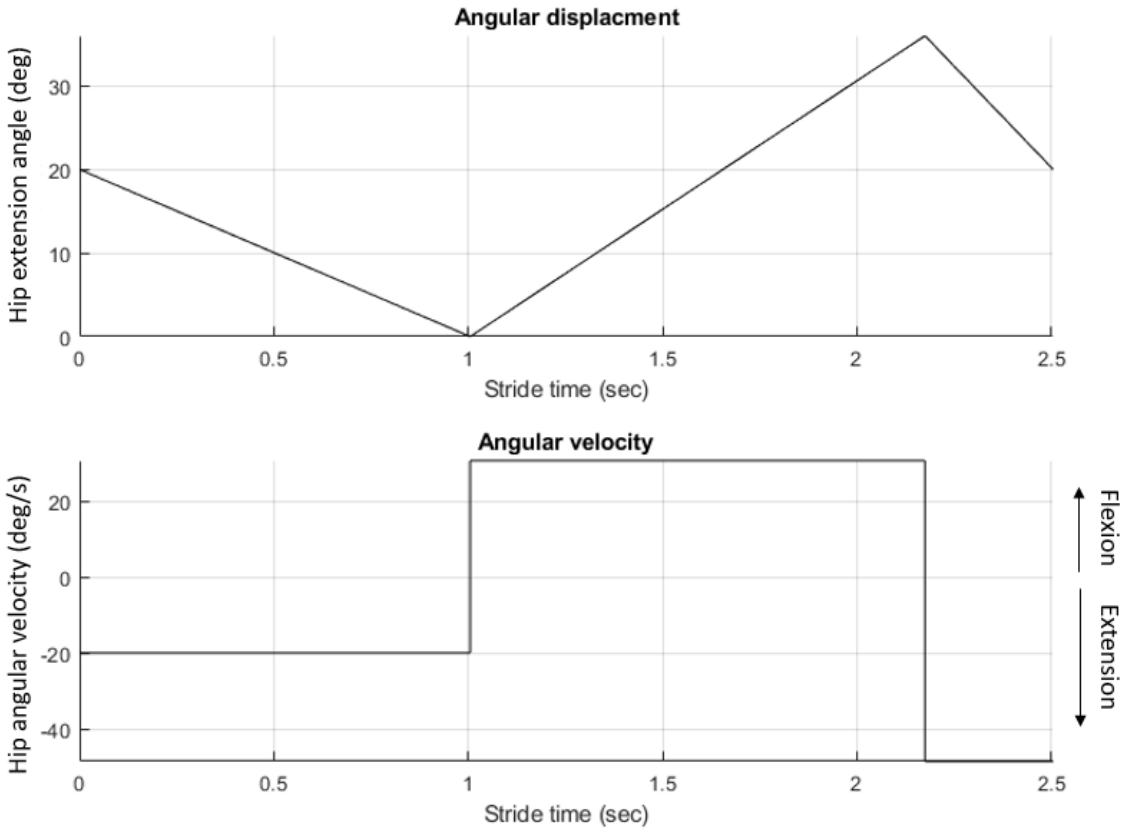

Figure 5.2 Hip angle and angular velocity profiles used for the IHK testing.

5.1.4 Test procedure

A 10 m walkway was prepared in a motion analysis lab for walking tests. Participants were asked to walk to the end of the walkway, turn, and walk back to record a minimum of 20 m of walking data for analysis. All participants had practiced walking on the IHK for at least one practice session before participating in the data recording session. The test procedure was as follows:

1. Power cycle the electronics.
2. Upload the angle position and angular velocity profiles to the hip joint electronics. Uploading the walking profiles does not put the joint into walking mode, the prosthesis remains idle.
3. Calibrate the neutral (mid-stance) hip joint angle to user preference.
4. Lift the HKAF off the ground and calibrate the load cells with zero load applied.
5. Start joint angle data, hip/waist angle data, and video recordings.

6. Initiate hip joint walking mode. A series of beeps informs the participant that walking mode is being initiated.
7. Record data for at least 20 m of walking.
8. Stop the hip joint walking mode.
9. Stop all recordings and save files.

5.1.5 Data collection and analysis

Using the TOHRC data logger application [47], a smartphone (Google Pixel 4a (2020)) was secured to the participant's lower back using a strap and holster to collect pelvic motion data, such as pelvic tilt, at a 100 Hz sampling rate. Videos of the test sessions were recorded at 60 frames per second using an iPhone 11 Pro (2019) while keeping the phone parallel to the prosthesis and having both the HKAF and the contralateral limb visible throughout the tests. Videos were analyzed using Kinovea video analysis software [48] to determine timestamps for heel-strikes and toe-offs for the HKAF and contralateral legs. The hip actuator (Össur Power Knee) and knee controller (Rheo Knee) both integrate hall-effect sensors for actuator angle measurement. Data from these sensors were collected at 50 Hz to determine hip and knee angles during testing.

The TOHRC data logger app, hip actuator angle sensor, and knee actuator angle sensor all produce separate output files with different start and end times. Video recordings, hip angle, and knee angle data were synchronised during terminal swing at the first stride of each test. The data point and video frame when the hip stopped flexing were used for hip synchronization. Knee data was aligned with video at the frame when the knee stopped extending. Eight consecutive strides were isolated and evaluated for each participant.

5.2 Results and discussion

The IHK was used in conjunction with the hip simulator across three separate tuning, practice, and recording sessions with no mechanical issues or faults. The electronics used in this evaluation were sufficient to demonstrate appropriate mechanical system function. However, a pre-commercial version will require optimized electronics and the development of an adaptive control system.

Table 5.3 provides a summary of the gait parameters obtained through 2D video analysis of eight consecutive strides for each participant. Average stride time for all

participants was 2.47 ± 0.14 seconds and cadence was 24.35 ± 1.41 steps per minute. These values are within the range of programmed values that were loaded into gait profile, which were 2.5 s stride time and 24 steps per minute cadence.

Stance and swing time analysis showed that participants employed different walking strategies. Participant A had a longer HKAF stance time (1.53 ± 0.11 s, 64% of stride) compared to participants B (1.22 ± 0.11 s, 49%) and C (1.26 ± 0.04 s, 51%) (i.e., participant A spent more time weight bearing on the HKAF). This was also reflected by participant A having 1.20 ± 0.12 s double support time compared to participants B (0.94 ± 0.07 s) and C (0.78 ± 0.07 s).

Table 5.3 Gait parameters determined through video analysis of eight consecutive strides for each participant, for prosthetic and intact limbs. Percentages indicate each gait parameter in proportion to stride time.

Participant		**A**	**B**	**C**	**Average**
Stride Time (s)		2.41 ± 0.08	2.51 ± 0.11	2.50 ± 0.21	2.47 ± 0.14
Stance Time (s)	**HKAF**	1.53 ± 0.11 (64%)	1.22 ± 0.11 (49%)	1.26 ± 0.04 (51%)	1.34 ± 0.16 (55%)
	Intact	2.13 ± 0.08 (88%)	2.23 ± 0.07 (89%)	2.02 ± 0.14 (81%)	2.12 ± 0.15 (86%)
Swing Time (s)	**HKAF**	0.93 ± 0.05 (39%)	1.29 ± 0.06 (50%)	1.24 ± 0.08 (51%)	1.15 ± 0.22 (46%)
	Intact	0.28 ± 0.02 (12%)	0.27 ± 0.01 (11%)	0.48 ± 0.06 (19%)	0.35 ± 0.11 (14%)
Double Support (s)		1.20 ± 0.12 (50%)	0.94 ± 0.07 (40%)	0.78 ± 0.07 (29%)	0.97 ± 0.20 (40%)
Cadence (steps/min)		24.93 ± 0.82	23.97 ± 1.06	24.15 ± 2.05	24.35 ± 1.41

Comparing the HKAF to the intact limb, gait was asymmetrical for all participants with average HKAF step time of 1.34 ± 0.16 s compared to 2.12 ± 0.15 s for the intact limb. Swing phase analysis showed gait asymmetry with the HKAF having an average swing time of 1.15 ± 0.22 s and the intact limb average swing time of 0.35 ± 0.11 s. Gait asymmetry was attributed to the use of a predefined gait profile for all three participants instead of an adaptive gait control system. Results showed that the participants had some

influence on step and swing speeds even with a static gait profile. During stance, participants B and C chose to use their bodyweight to force the hip to move faster and end stance phase earlier, while participant A chose to initiate heel contact earlier than the gait profile was programmed to in order to have a small period of time to prepare for the next stride before the gait profile entered stance phase.

Table 5.4 shows hip and knee angle ranges of motion. The IHK hip average ROM was 36.57 ± 3.23° with an average hip extension of -5.16 ± 4.98° and an average hip flexion of 31.41 ± 2.44°. The observed range of motion meets the programmed gait profile value of 36°, while hip extension (programmed at 0°) and flexion (programmed at 36°) values did not. This discrepancy may be caused by the control system undershooting the swing phase motion or participants forcing the hip to move in a motion they found more comfortable.

Table 5.4 IHK hip and knee range of motion for eight consecutive strides for each participant, measured using sensor data from the hip joint motor and the Rheo Knee angle sensor.

	Participants			**Average**
	A	**B**	**C**	
Max hip extension (deg)	-1.23 ± 0.20	-2.22 ± 0.29	-12.03 ± 0.23	-5.16 ± 4.98
Max hip flexion (deg)	33.93 ± 1.01	31.60 ± 0.82	28.70 ± 1.48	31.41 ± 2.44
Hip range of motion (deg)	35.16 ± 1.11	33.82 ± 0.80	40.73 ± 1.34	36.57 ± 3.23
Max knee extension (deg)	-1.87 ±0.02	-1.77 ± 0.05	-1.97 ± 0.04	-1.87 ± 0.09
Max knee flexion (deg)	30.98 ± 4.04	57.42 ± 3.57	38.23 ± 9.99	42.21 ± 13.00
Knee range of motion (deg)	32.85 ± 4.02	59.19 ± 3.58	40.20 ± 10.01	44.08 ± 12.95

Another potential cause for the flexion deficiency is that toe drag was observed during swing, which would have produced resistance to flexion during swing. Participants

B and C experienced toe drag throughout data recording, which explains their results not matching the programmed hip ROM value. These results also showed that participant C had a different walking strategy than the other participants, since he chose to force the hip up to -12.49° of extension compared to -1.58° for participant A and -2.55° for participant B. This is believed to be caused by participant C choosing a gait strategy that he found more comfortable at the time of testing.

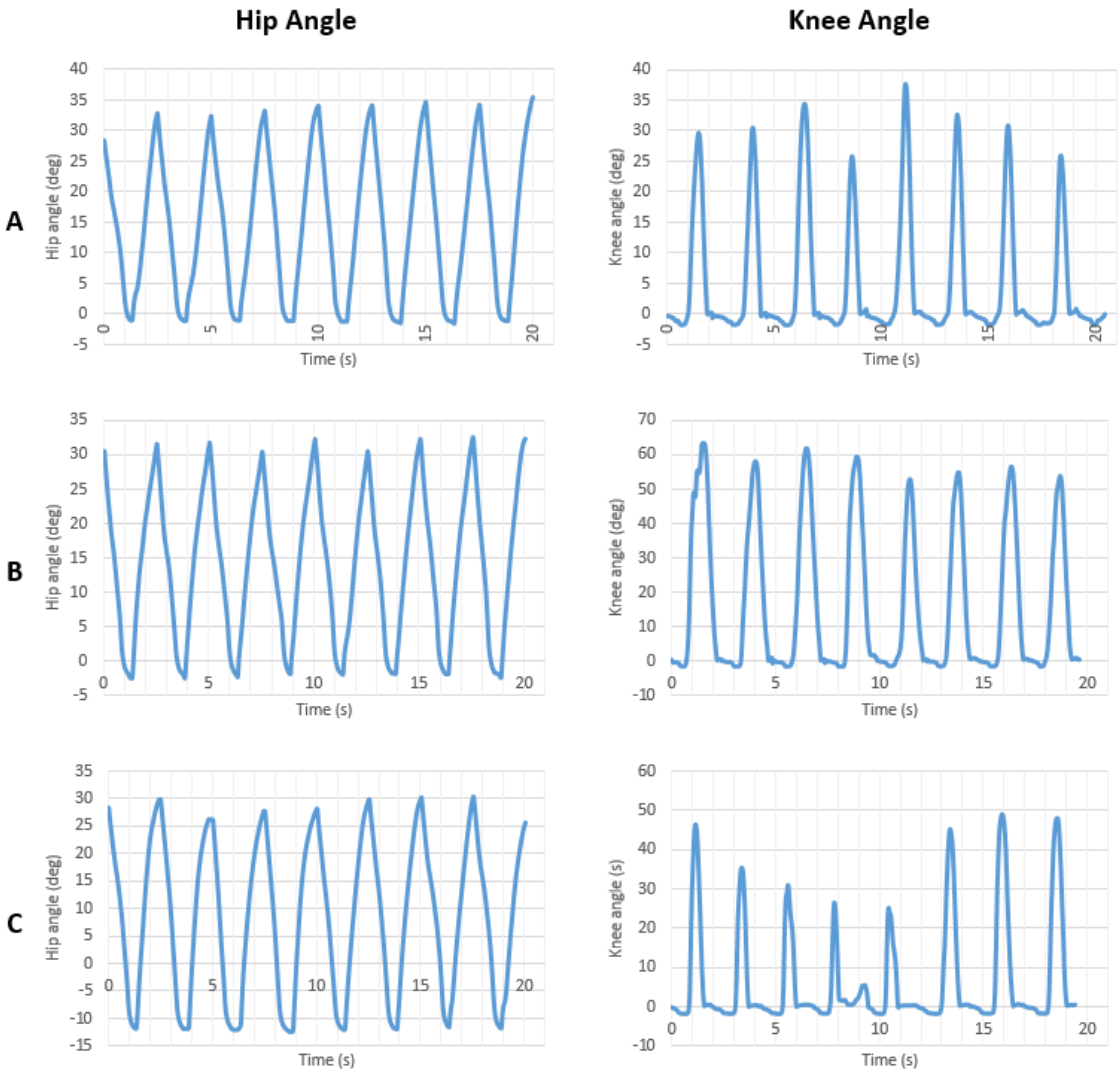

Figure 5.3 Hip angle versus time and knee angle versus time (s) for eight consecutive steps for participants A, B, and C.

The knee joint had an average ROM of 51.95 ± 12.78°, with a maximum average flexion of 50.00 ± 12.83°. Although this iteration of the IHK knee joint uses mostly unmodified Rheo Knee 3 electronics and control system, the knee correctly switched between stance and swing modes.

Hip angle versus time and knee angle versus time for all three participants are shown in Figure 5.3. Note that participant C had a slight stumble during his fourth step, which is visible in the knee angle versus time graph.

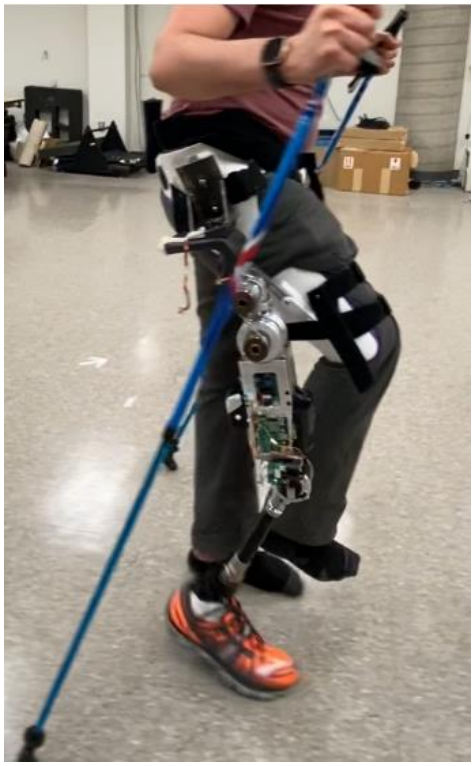

Figure 5.4 Toe drag observed during swing phase.

Video analysis showed that participants B and C had difficulty achieving toe clearance during swing, showing an excessive amount of toe drag (Figure 5.4). This is believed to be caused by the Rheo knee actuator extension spring and controls not decreasing flexion resistance early enough in terminal stance and swing initiation. The extension spring in the Rheo actuator was designed with the assumption that the Rheo knee electronics and battery would be located in the shank, making the shank heavier. Since the IHK shifts the knee electronics and battery weight to the thigh, the shank is lighter and the torsion spring may provide too much extension torque, causing the toe to drag on the floor. Another potential cause of toe drag is that the knee control system is providing too much resistance to knee flexion during early swing. It is believed that participant A experienced little toe drag due to his experience walking on the hip simulator, allowing him to correctly make the gait adjustments to allow the foot to clear the ground.

Pelvic tilt and pelvic obliquity data were collected using a smartphone placed on the participant's lower back, just above the hip simulator. An average pelvic tilt range of 16.02 ± 3.40° was observed across participants. In comparison, the able-bodied pelvic tilt range is 4.3 ± 1.1° [49] and the pelvic tilt range of the Ottobock Helix3D was measured to be 20 ± 4° [9]. An average pelvic obliquity range of 8.39 ± 1.98° was observed across all participants, compared to an able-bodied range of 7.4 ± 2.5° [49].

Results show that pelvic tilt range of the IHK was did not substantially improve upon the results of the Helix3D, and that there was more pelvic tilt motion compared to an able-bodied person. Walking with the simulator instead of a socket, that provides a better interface to the human body, likely also contributed to the pelvic tilt range with the IHK. The IHK range of pelvic obliquity was within range of able-bodied people. The next iteration of the IHK that implements the adaptive gait control system will likely improve upon the pelvic tilt range of the IHK to for more natural gait.

The mechanical tests and functionality tests with able-bodied participants demonstrated that the powered HKAF prosthesis is safe for next-phase evaluation with HD or HP amputees. The goal of this research was to test the IHK mechanical aspects when used for level walking; however, data from able-bodied participants wearing a hip simulator that positions the HKAF prosthesis laterally to the pelvis instead of directly in front of the pelvis may differ from people with hip-level amputations and a good fitting prosthesis. Mounting the IHK to the hip simulator is not as rigid as direct mounting to a socket; therefore, some movement of the prosthesis relative to the pelvis may occur as the hip simulator stretches and flexes while under load. Additionally, the lateral mounting point results in the prosthesis not being directly below the body center of mass, creating a cantilever effect on the prosthesis. As a result, the loads applied to the IHK could differ from loads expected by amputee users. The laterally mounted HKAF may also result in able-bodied users developing different gait strategies than amputee users, to compensate for differences between the simulator and socket systems.

The collected data from user testing is only representative of able-bodied users using a hip simulator, however it does provide design insights for future iterations of the IHK that will be tested with amputee users. For example, the data showed that each participant chose a different and unique walking strategy. This observation can help guide

IHK control system development since it shows that a control system should not force a static gait pattern onto users but should adapt to the user and give the user some freedom to override the hip joint to let users to walk in a way they find most comfortable. User testing also showed that the IHK was able to meet several of the outlined design criteria: the IHK was able to sustain walking loads, loads were not transferred to the electronics, loads measurements provided sufficient accuracy for the joint control systems, and the IHK was adjustable to different users.

Chapter 6: Conclusions and Future Work

6.1 Conclusion

In this thesis, an integrated thigh unit was designed with a powered hip and microprocessor controlled knee and evaluated to study the mechanical aspect of this device within a HKAF prosthesis for use by hip amputees.

The chassis design was guided by a set of criteria based on anthropometric data, prosthetist guidance, and safety standards for lower limb prostheses. A summary of the defined criteria and the achieved criteria are given in Table 6.1. Of note, the defined safety and structural stability criteria were successfully met. Several criteria relating to the electronics and control system of the device were not met and are the subject of ongoing work.

Table 6.1 IHK design criterion and results

Criteria	Requirement	Tested result
Thigh length accommodates up to the 5th percentile of the population or better	IHK minimum configurable length ≤ 42 cm	Pass. Shortest configurable length determined to be 41.7 cm, however only one pyramid adapter can be used for adjustments between chassis and powered hip.
Total IHK mass is equivalent to or less than the combined mass of Rheo Knee 3 and Power Knee.	IHK mass ≤ 4.8 kg	Fail. Measured IHK mass was about 5 kg. The tested IHK required individual batteries and electronics for each joint. Future iterations could meet the weight requirement through improved joint integration, electronics optimization, and one battery.
Rheo Knee 3 actuator is fully integrated into the structure of the chassis	Joint is fully controllable and provides rotational resistance	Pass. Actuator was functional and provided variable resistance to the knee joint based on gait parameters
Chassis is modular and allows more than one IHK configuration with different hip components	Chassis can accept different powered hip joints	Pass. Two different powered hip joint designs were tested with the chassis

The IHK structure contains and protects the electronics	Electronics are in the chassis structure and no force is transmitted to the electronics	Fail. Later electronic development resulted in electronics needing more space than expected, and can no longer fit in the chassis electronics compartment.
The IHK must be structurally safe and withstand typical loads experienced during walking	Chassis passes ISO-10328:2016 standards for lower limb prostheses	Pass. Chassis passed ISO-10328:2016 static and cyclic tests in simulations, and passed static proof load test in P5 LCI in bench tests
Chassis provides reliable and accurate load data to the control system	Applied load on the chassis is reliable and repeatable	Pass. Testing on an Instron machine showed that load data was linear and repeatable
MPC hip and knee joints are electronically integrated, and share sensor data, battery power, and processing power	Both joints are controlled by one microcontroller, share a battery, and share all sensor data	Partial pass. Joints share chassis load data, but have individual microprocessors and batteries, and do not share individual joint data (such as joint angle and joint torque). Further work is being completed on addressing this issue.

The IHK was assembled with a novel powered hip design and a preliminary control system. It was then tested on a hip prosthesis simulator to allow able-bodied study participants to walk on the IHK.

6.2 Future Work

Several points of improvement were noted during bench testing and user testing of the chassis. These future improvements should make the chassis easier to use and would hide the exposed electronics. Other future work includes testing different actuator control systems and sensor configurations.

6.2.1 Electronics compartment

The chassis design assumed both hip and knee joints, as well as the strain gauge sensors, could be operated using the Power Knee control and power boards alone. Electronics development, which occurred after the chassis had been sent for manufacturing, showed that operating all electronics using the Power Knee electronics alone would have many challenges and would greatly delay the mechanical performance evaluation. As a

result, more electronic control boards than expected were used in the project, resulting in some electronics being outside of the chassis structure. Future work on optimising device electronics should allow one set of control and power boards to reside within subsequent chassis versions.

6.2.2 Shared joint angle sensor data and synergistic gait control

IHK synergistic gait control could potentially result in better movement across a variety of mobility scenarios. The chassis design facilitates hip and knee units working together by providing the infrastructure for shared sensor input, electronics, and battery power. In the current prototype, only chassis load data was shared between the knee and hip control systems. Future IHK development should focus on hip and knee joint control integration to allow for unrestricted sensor data sharing and synergistic control.

6.2.3 Strain inducing geometries

In the current chassis design, priority was given to ease of manufacturing and modularity. Strain gauge placement was chosen by locating chassis flat areas that displayed the highest strain measurements in simulations. Future chassis revisions could include strain inducing geometries to reduce the amount of amplification and increase strain gauge sensitivity.

6.2.4 Strain gauge calibration

In the current chassis design, any changes to strain gauge configuration and any new manufactured chassis units need to undergo hour-long calibration on an Instron machine to calibrate the force measurement values. A more refined and faster calibration process could be developed to reduce the downtime of chassis units between configuration changes.

6.2.5 Improved testing/calibration components

For the bench testing and calibration processes, a custom aluminum part, the P5 LCI test rig, was created to direct the applied test load in the ISO 10328 defined test load direction. This custom part was also used during strain gauge calibration. During calibration, artifacts were observed in the collected load data in trials conducted near the end of the calibration session. P5 LCI test rig analysis showed deformation and denting of the loading surface, which is believed to be one of the causes of data artifacts (Figure 4.7). If future chassis continue to use the same or similar calibration procedures as defined in

Section 4.2, a new P5 LCI test rig should be manufactured using a wear resistant material to reduce the effect of wear on chassis calibration.

6.2.6 Improve Power Knee battery holding parts

During testing, the chassis battery holding 3D printed components could not keep the battery in place if the chassis experienced multiple movements when testing battery fitment during assembly. The battery would slowly loosen until it would either fall out of the chassis or lose engagement with PCB pins connecting it to the electronics. To avoid the risk of the battery falling out of the chassis during testing, the battery was held in place with tape and rubber bands during user testing. Future chassis revisions should experiment with different battery holding designs to ensure the battery will stay secure in the chassis. Testing has already begun on a new iteration of battery holding parts.

6.2.7 Improve knee motion

User testing of the IHK showed that two of the three participants had difficulties achieving toe/foot clearance during swing. No conclusion was made on the exact cause of the toe drag, however potential causes include the knee actuator providing too much resistance to flexion in early swing and the Rheo actuator extension spring providing too much extension torque. Further testing should be conducted to determine the cause(s) of toe drag and develop solutions to improve user gait with the IHK.

6.2.8 Amputee user testing

The mechanical tests and functional tests with able-bodied participants demonstrated that the powered HKAF prosthesis is safe for next phase evaluation with hip disarticulation or hemipelvectomy amputees. Future work will involve testing with amputee participants after the adaptive gait control system has been completed.

References

[1] E. Ludwigs, A. Kannenberg, and D. Wüstefeld, "Evaluation of the Benefits of a New Prosthetic Hip Joint System in Activities of Daily Function in Patients after Hip Disarticulation or Hemipelvectomy," *JPO: Journal of Prosthetics and Orthotics*, vol. 25, no. 3, p. 118, Jul. 2013, doi: 10.1097/JPO.0b013e31829afc1c.

[2] A. Fernández and J. Formigo, "Are Canadian Prostheses Used? A Long-Term Experience," *Prosthet Orthot Int*, vol. 29, no. 2, pp. 177–181, Aug. 2005, doi: 10.1080/03093640500217208.

[3] D. G. Shurr, T. M. Cook, J. A. Buckwalter, and R. R. Cooper, "Hip Disarticulation: A Prosthetic Follow-Up," *Journal of the American Orthotic and Prosthetic Association*, vol. 37, no. 3, pp. 50–57, 1983.

[4] T. Chin, H. Oyabu, Y. Maeda, I. Takase, and K. Machida, "Energy Consumption During Prosthetic Walking and Wheelchair Locomotion by Elderly Hip Disarticulation Amputees," *American Journal of Physical Medicine & Rehabilitation*, vol. 88, no. 5, p. 399, May 2009, doi: 10.1097/PHM.0b013e3181a0dbe2.

[5] M. J. Highsmith, J. T. Kahle, S. L. Carey, D. J. Lura, R. V. Dubey, and W. S. Quillen, "Kinetic Differences Using a Power Knee and C-Leg While Sitting Down and Standing Up: A Case Report," *JPO: Journal of Prosthetics and Orthotics*, vol. 22, no. 4, pp. 237–243, Oct. 2010, doi: 10.1097/JPO.0b013e3181f46b65.

[6] R. Fluit, E. Prinsen, S. Wang, and H. Van Der Kooij, "A comparison of control strategies in commercial and research knee prostheses," *IEEE Transactions on Biomedical Engineering*, pp. 1–1, 2019, doi: 10.1109/TBME.2019.2912466.

[7] K. R. Kaufman *et al.*, "Gait and balance of transfemoral amputees using passive mechanical and microprocessor-controlled prosthetic knees," *Gait & Posture*, vol. 26, no. 4, pp. 489–493, Oct. 2007, doi: 10.1016/j.gaitpost.2007.07.011.

[8] K. R. Kaufman, J. A. Levine, R. H. Brey, S. K. McCrady, D. J. Padgett, and M. J. Joyner, "Energy Expenditure and Activity of Transfemoral Amputees Using Mechanical and Microprocessor-Controlled Prosthetic Knees," *Archives of Physical Medicine and Rehabilitation*, vol. 89, no. 7, pp. 1380–1385, Jul. 2008, doi: 10.1016/j.apmr.2007.11.053.

[9] E. Ludwigs, M. Bellmann, T. Schmalz, and S. Blumentritt, “Biomechanical Differences between Two Exoprosthetic Hip Joint Systems during Level Walking,” *Prosthet Orthot Int*, vol. 34, no. 4, pp. 449–460, Dec. 2010, doi: 10.3109/03093646.2010.499551.

[10] M. Windrich, M. Grimmer, O. Christ, S. Rinderknecht, and P. Beckerle, “Active lower limb prosthetics: a systematic review of design issues and solutions,” *BioMedical Engineering OnLine*, vol. 15, no. 3, p. 140, Dec. 2016, doi: 10.1186/s12938-016-0284-9.

[11] B. Imam, W. C. Miller, H. C. Finlayson, J. J. Eng, and T. Jarus, “Incidence of lower limb amputation in Canada,” *Can J Public Health*, vol. 108, no. 4, pp. e374–e380, Nov. 2017, doi: 10.17269/cjph.108.6093.

[12] Y. Ueyama, T. Kubo, and M. Shibata, “Robotic hip-disarticulation prosthesis: evaluation of prosthetic gaits in a non-amputee individual,” *Advanced Robotics*, vol. 34, no. 1, pp. 37–44, Jan. 2020, doi: 10.1080/01691864.2019.1705908.

[13] V. Struchkov and J. G. Buckley, “Biomechanics of ramp descent in unilateral trans-tibial amputees: Comparison of a microprocessor controlled foot with conventional ankle–foot mechanisms,” *Clinical Biomechanics*, vol. 32, pp. 164–170, Feb. 2016, doi: 10.1016/j.clinbiomech.2015.11.015.

[14] P. Yari, P. U. Dijkstra, and J. H. Geertzen, “Functional outcome of hip disarticulation and hemipelvectomy: a cross-sectional national descriptive study in the Netherlands,” *Clin Rehabil*, vol. 22, no. 12, pp. 1127–1133, Dec. 2008, doi: 10.1177/0269215508095088.

[15] M. Spoden, U. Nimptsch, and T. Mansky, “Amputation rates of the lower limb by amputation level – observational study using German national hospital discharge data from 2005 to 2015,” *BMC Health Serv Res*, vol. 19, no. 1, p. 8, Jan. 2019, doi: 10.1186/s12913-018-3759-5.

[16] S. Hussain, S. Shams, and S. Khan, “Impact of Medical Advancement: Prostheses,” in *Computer Architecture in Industrial, Biomechanical and Biomedical Engineering*, BoD – Books on Demand, 2019, pp. 9–28. doi: 10.5772/intechopen.86602.

[17] C. A. Bell, “Canadian Hip Disarticulation Prosthesis,” *Orthopedic & Prosthetic Appliance Journal*, vol. 10, pp. 35–39, Mar. 1956.

[18] V. S. Urrutia, “The swing phase of hip disarticulation amputee walking: An analysis of walking constraints and methodological implications for gait analysis - ProQuest,” Dissertation, Northwestern University, 1996. Accessed: Nov. 07, 2021. [Online]. Available: https://www.proquest.com/openview/412ecf9c8b8e362689a30e1e4db36e93/1?pq-origsite=gscholar&cbl=18750&diss=y

[19] “Modular Single Axis Hip Joint | Hips | Lower Limb Prosthetics | Prosthetics | Ottobock CA Shop.” https://shop.ottobock.ca/en/Prosthetics/Lower-Limb-Prosthetics/Hips/Modular-Single-Axis-Hip-Joint/p/7E5~5L (accessed Nov. 09, 2021).

[20] “7E7 Instructions for use.” Ottobock, Jul. 09, 2020. [Online]. Available: https://shop.ottobock.us/store/medias/647G130-all-INT-16-2102w-4495081-en.pdf?context=bWFzdGVyfHJvb3R8MTIzMDE2N3xhcHBsaWNhdGlvbi9wZGZ8aDM0L2g2MS84OTMwMTQ2NzEzNjMwLnBkZnwzN2JmYTE0NzE0NWM0NzU3NTZhMjc3MWYxZmUwOGM0ZmJmNWNkODMwMjVmNjkxMzQyNDlkNzUzODQzOGE3MDU5

[21] “Modular Hip Joint Free Mot. Titan | Hips | Lower Limb Prosthetics | Prosthetics | Ottobock CA Shop.” https://shop.ottobock.ca/en/Prosthetics/Lower-Limb-Prosthetics/Hips/Modular-Hip-Joint-Free-Mot-Titan/p/7E7 (accessed Nov. 07, 2021).

[22] “Hydraulic Hip Joint | Hips | Lower Limb Prosthetics | Prosthetics | Ottobock CA Shop.” https://shop.ottobock.ca/en/Prosthetics/Lower-Limb-Prosthetics/Hips/Hydraulic-Hip-Joint/p/7E9 (accessed Nov. 09, 2021).

[23] “7E10 Helix3D Intructions for use (Qualified Personnel).” Ottobock, Sep. 02, 2021.

[24] “Helix3D Hip Joint, right,” *Ottobock*. https://shop.ottobock.us/Prosthetics/Lower-Limb-Prosthetics/Hips/Helix3D-Hip-Joint,-right/p/7E10~5R (accessed Oct. 17, 2019).

[25] “Linx - Integrated Limb System - Blatchford US & Canada,” *Blatchford US & Canada - Mobility Made Possible*. https://www.blatchfordus.com/products/linx/ (accessed Feb. 26, 2022).

[26] Z. M. Abdulhasan, “Impact of combined microprocessor control of the prosthetic knee and ankle on gait termination in unilateral trans-femoral amputees. Limb mechanical work performed on centre of mass to terminate gait on a declined surface

using linx prosthetic device," Doctor of Philosophy, University of Bradford, Bradford, West Yorkshire, England, 2018. Accessed: Feb. 27, 2022. [Online]. Available: https://bradscholars.brad.ac.uk/handle/10454/16906

[27] Z. M. Abdulhasan, A. J. Scally, and J. G. Buckley, "Gait termination on a declined surface in trans-femoral amputees: Impact of using microprocessor-controlled limb system," *Clinical Biomechanics*, vol. 57, pp. 35–41, Aug. 2018, doi: 10.1016/j.clinbiomech.2018.05.015.

[28] D. A. Winter, *The Biomechanics and Motor Control of Human Gait*. Waterloo, Ontario, Canada: University of Waterloo Press, 1987.

[29] D. A. Winter, Ed., *Biomechanics and Motor Control of Human Movement*, 4th ed. John Wiley & Sons, Inc., 2009.

[30] W. Pirker and R. Katzenschlager, "Gait disorders in adults and the elderly: A clinical guide," *Wiener klinische Wochenschrift*, vol. 129, Oct. 2016, doi: 10.1007/s00508-016-1096-4.

[31] M. T. Karimi, M. Kamali, H. Omar, and J. Mostmand, "Evaluation of Gait Performance of a Hemipelvectomy Amputation Walking with a Canadian Prosthesis," *Case Reports in Orthopedics*, vol. 2014, p. e962980, Apr. 2014, doi: 10.1155/2014/962980.

[32] B. L. Schnall, B. S. Baum, and A. M. Andrews, "Gait Characteristics of a Soldier With a Traumatic Hip Disarticulation," *Physical Therapy*, vol. 88, no. 12, pp. 1568–1577, Dec. 2008, doi: 10.2522/ptj.20070337.

[33] C. D. Fryar, Q. Gu, C. L. Ogden, and K. M. Flegal, "Anthropometric reference data for children and adults; United States, 2011-2014," *Vital and health statistics. Series 3DHHS publication ; no. (PHS)*, p. 46, Aug. 2016.

[34] "Power Knee Instructions for Use." Össur. Accessed: Sep. 07, 2021. [Online]. Available: https://media.ossur.com/image/upload/v1587727308/product-documents/global/PN20033/IFUS/PN20033_Power_Knee.pdf

[35] "Rheo Knee Instructions for Use." Össur. Accessed: Sep. 07, 2021. [Online]. Available: https://media.ossur.com/image/upload/v1625231201/product-documents/global/PN20224/IFUS/PN20224_RHEO_Knee.pdf

[36] “ISO 10328:2016 - Prosthetics — Structural testing of lower-limb prostheses — Requirements and test methods.” International Organization for Standardization, Jun. 2016. Accessed: Aug. 02, 2021. [Online]. Available: https://www.iso.org/cms/render/live/en/sites/isoorg/contents/data/standard/07/02/70205.html

[37] T. Reist, J. Andrysek, and W. Cleghorn, “Topology Optimization of an Injection Moldable Prosthetic Knee Joint,” *Computer-Aided Design & Applications CAD Solutions*, vol. 7, pp. 247–256, Jan. 2010, doi: 10.3722/cadaps.2010.247-256.

[38] “ISO 898-1:2013 - Mechanical properties of fasteners made of carbon steel and alloy steel — Part 1: Bolts, screws and studs with specified property classes — Coarse thread and fine pitch thread.” International Organization for Standardization, Jan. 2013. Accessed: Aug. 02, 2021. [Online]. Available: https://www.iso.org/cms/render/live/en/sites/isoorg/contents/data/standard/06/06/60610.html

[39] “BS EN 1993-1-8:2005 Eurocode 3. Design of steel structures Design of joints.” European Union, 2005. Accessed: Aug. 04, 2021. [Online]. Available: https://www.en-standard.eu/bs-en-1993-1-8-2005-eurocode-3-design-of-steel-structures-design-of-joints/

[40] E. Standards, “BS EN 1993-1-1:2005+A1:2014 Eurocode 3. Design of steel structures General rules and rules for buildings.” European Union, 2005. Accessed: Aug. 20, 2021. [Online]. Available: https://www.en-standard.eu/bs-en-1993-1-1-2005-a1-2014-eurocode-3-design-of-steel-structures-general-rules-and-rules-for-buildings/

[41] “Screw Thread Standards for Federal Service - Section 2 - Unified Inch Screw Threads - UN and UNR Forms, FED-STD-H28/2B.” Federal Supply Services, General Services Administration, Washington, DC., Apr. 20, 1984.

[42] “ASM Material Data Sheet.” http://asm.matweb.com/search/SpecificMaterial.asp?bassnum=MA2024T4 (accessed Aug. 20, 2021).

[43] “Easy & precise height adjustment — no cutting needed.. Ossur.com.” https://www.ossur.com/en-ca/prosthetics/adapters/height-adjustable-pylon (accessed Oct. 26, 2022).

[44] “Adapters for Prosthetic Feet, Knees & Sockets. Ossur.com.” https://www.ossur.com/en-ca/prosthetics/adapters (accessed Nov. 01, 2022).

[45] A. Fanous, M. Botros, H. Gholizadeh, N. Baddour, and E. D. Lemaire, “Design and evaluation of a hip prosthesis simulator: A technical note,” *Prosthetics and Orthotics International*, pp. 10–1097, Jan. 2023, doi: 10.1097/PXR.0000000000000208.

[46] “Pro-Flex® XC Prosthetic Foot by Össur.” https://www.ossur.com/en-ca/prosthetics/feet/pro-flex-xc (accessed Feb. 12, 2023).

[47] E. D. Lemaire, M. D. Tundo, and N. Baddour, “Evaluation of a Smartphone-based Human Activity Recognition System in a Daily Living Environment,” *J Vis Exp*, no. 106, p. 53004, Dec. 2015, doi: 10.3791/53004.

[48] “Kinovea.” https://www.kinovea.org/ (accessed Feb. 14, 2023).

[49] C. L. Lewis, N. M. Laudicina, A. Khuu, and K. L. Loverro, “The Human Pelvis: Variation in structure and function during gait,” *Anat Rec (Hoboken)*, vol. 300, no. 4, pp. 633–642, Apr. 2017, doi: 10.1002/ar.23552.

Appendix A: ISO Loading Forces

Table A.1 provides the loads for ISO-10328:2016 P5 static loading tests. Table A.2 provides loads for cyclic testing.

Table A.1: ISO-10328:2016 P5 load levels for different static load tests [36].

Loading Test	Load Condition LCI	Load Condition LCII
Ultimate Static Load Test (N)	4480	4025
Proof Load Test (N)	2240	2013
Maximum Twisting Moments (N*m)	50	

Table A.2: ISO-10328:2016 P5 load levels for cyclic load tests [36].

Test Description	Load Condition LCI	Load Condition LCII
Minimum Cyclic Load (N)	50	
Maximum Cyclic Load (N)	1330	1200
Prescribed Number of Cycles	$3 * 10^6$	
Final Static Force (N)	2240	2013

Appendix B: Bolt Analysis References

Ultimate tensile failure reference:

The proof load strengths and stress areas of metric coarse pitch threads can be obtained from the ISO898:2013 standard which details the mechanical properties of bolts and screws.

Table B.1 Proof load values and stress areas for class 12.9 bolts as defined by Table 5 of ISO898:2013 [38].

Thread	**Class 12.9 Proof load (N)**	**Nominal stress area (mm^2)**
M3	4880	5.03
M4	8520	8.78
M5	13800	14.2
M6	19500	20.1

Shear failure references:

Shear resistance equation as defined by Table 3.4 of EN 1993-1-8:2005 [39]:

$$F_{V,Rd} = \frac{\alpha_V f_{ub} A}{\gamma_{M2}} \tag{B.1}$$

In this equation,

- α_V = multiplying factor
- f_{ub} = ultimate tensile strength of the bolt
- A = tensile stress area of the bolt
- γ_{M2} = partial factor for resistance of cross-section in tension

The multiplying factor is defined as:

- $a_V = 0.6$ for classes 4.6, 5.6, and 8.8
- $a_V = 0.5$ for classes 4.8, 5.8, 6.8, and 10.9

Since the standard does not provide a multiplying factor for class 12.9 bolts, the smallest given multiplying factor ($a_V = 0.5$) was used for calculations, since it will provide a smaller shear resistance value.

The ultimate tensile strength of aluminum 2024 is approximately 284MPa [42].

The stress areas defined by ISO898:2013 (Table B.1) are used.

The partial factor for resistance of cross-sections in tension to fracture is defined by EN 1993-1-1:2005 as $\gamma_{M2} = 1.25$ [40].

Bolt thread integrity references (internal and external threads):

Table II.B.1 from FED-STD-H28/2B provides formulas to determine thread shear areas [41]. Internal thread shear area is defined by the following equation:

$$A_s = \pi n L_e d_{min} \left[\frac{1}{2n} + 0.57735(d_{min} - D_{2max})\right] \quad \text{(B.2)}$$

External thread shear area is defined by the following equation:

$$A_{s,external} = \pi n L_e D_{1max} \left[\frac{1}{2n} + 0.57735(d_{2min} - D_{1max})\right] \quad \text{(B.3)}$$

In these equations,

- A_s = internal thread shear area
- $A_{s,external}$ = external thread shear area
- n = number of threads per unit length (1/pitch)
- L_e = engagement length of threads
- d_{min} = minimum value of the major diameter of the external thread
- d_{2min} = minimum value of the pitch diameter of the external thread
- D_{1max} = maximum value of the minor diameter of the internal thread
- D_{2max} = maximum value of the pitch diameter of the internal thread

Rearranging equations (B.2) and (B.3), an equation to determine engagement length of the bolt can be determined. The calculated engagement length can be used to determine if a bolt has sufficient length to withstand the expected loads that will act on it. The following equation provides the required engagement length of an internal thread, derived from equation (B.2).

$$L_e = \frac{A_s}{\pi n d_{min} \left[\frac{1}{2n} + 0.57735(d_{min} - D_{2max})\right]} \quad \text{(B.4)}$$

The required thread shear area to resist tensile loading on the bolt can be calculated by dividing the tensile load acting on the bolt by the shear yield strength of the thread material:

$$A_s = \frac{F_b}{\sigma_{sy}} \tag{B.5}$$

where

- A_s = internal thread shear area
- F_b = tensile load acting on the bolt
- σ_{sy} = shear yield strength of the thread material

Substituting equation (B.5) into (B.4), an equation to determine the required engagement length of an internal thread can be derived given thread dimensions, thread material properties, and load acting on the threads.

$$L_e = \frac{F_b}{\sigma_{sy}\pi n d_{min}\left[\frac{1}{2n} + 0.57735(d_{min} - D_{2max})\right]} \tag{B.6}$$

An equation can also be derived for engagement length of external threads by completing a similar equation derivation using equation (B.3).

Appendix C: Purchased Component Specifications

Bolts and connectors were purchased through the McMaster-Carr online store (Table C.1). Aluminum 2024 was used for chassis parts. The Power Knee battery and control board, and the Rheo Knee 3 actuator and control boards were provided by Össur.

Table C.1 Connector names and McMaster-Carr part numbers.

Connector name	Part number
Black-oxide alloy steel socket head screw M5x0.8, 16mm	91290A232
Black-oxide alloy steel socket head screw M5x0.8, 12mm	91290A228
Black-oxide alloy steel socket head screw M3x0.5, 18mm	91290A121
Black-oxide alloy steel socket head screw M4x0.7, 16mm	91290A154
Black-oxide alloy steel socket head screw M3x0.5, 14mm	91290A119
Black-oxide alloy steel socket head screw M6x1.0, 15mm	91290A320

Appendix D: Electronics Design

Table D.1 Data collection system bill of materials.

Name	Schematic Designator	Qty.	Manufacturer Part Number	Manufacturer
BH-18650-B1BA002	BT1	1	BH-18650-B1BA002	MYOUNG(美阳)
ISO1541D	I2C	1	ISO1541D	Texas Instruments
LED-0603_R	LED1	1	19-217/R6C-AL1M2VY/3T	EVERLIGHT(台湾亿光)
LED-0603_B	LED2	1	19-217/BHC-ZL1M2RY/3T	EVERLIGHT(台湾亿光)
Generic 1k resistor	R1,R2	2	N/A	N/A
ISO7721DR	SPI1,UART	2	ISO7721DR	Texas Instruments
ISO7720DR	SPI2	1	ISO7720DR	Texas Instruments
SK-12D02-VG5	SW1	1	SK-12D02-VG5	Rectangular Connectors - Contacts
ESP32 DEVKIT V1	U1	1	ESP32-DevKit-V1	Espressif
BNO055	U2	1		
EVAL-AD7124-8	U2	1	EVAL-AD7124-8	ANALOG Devices
Strain Gauge Full Wheatstone Bridge	U3,U4	2	BF350-3AA	DAOKI
Generic SD card reader	M2	1	N/A	N/A

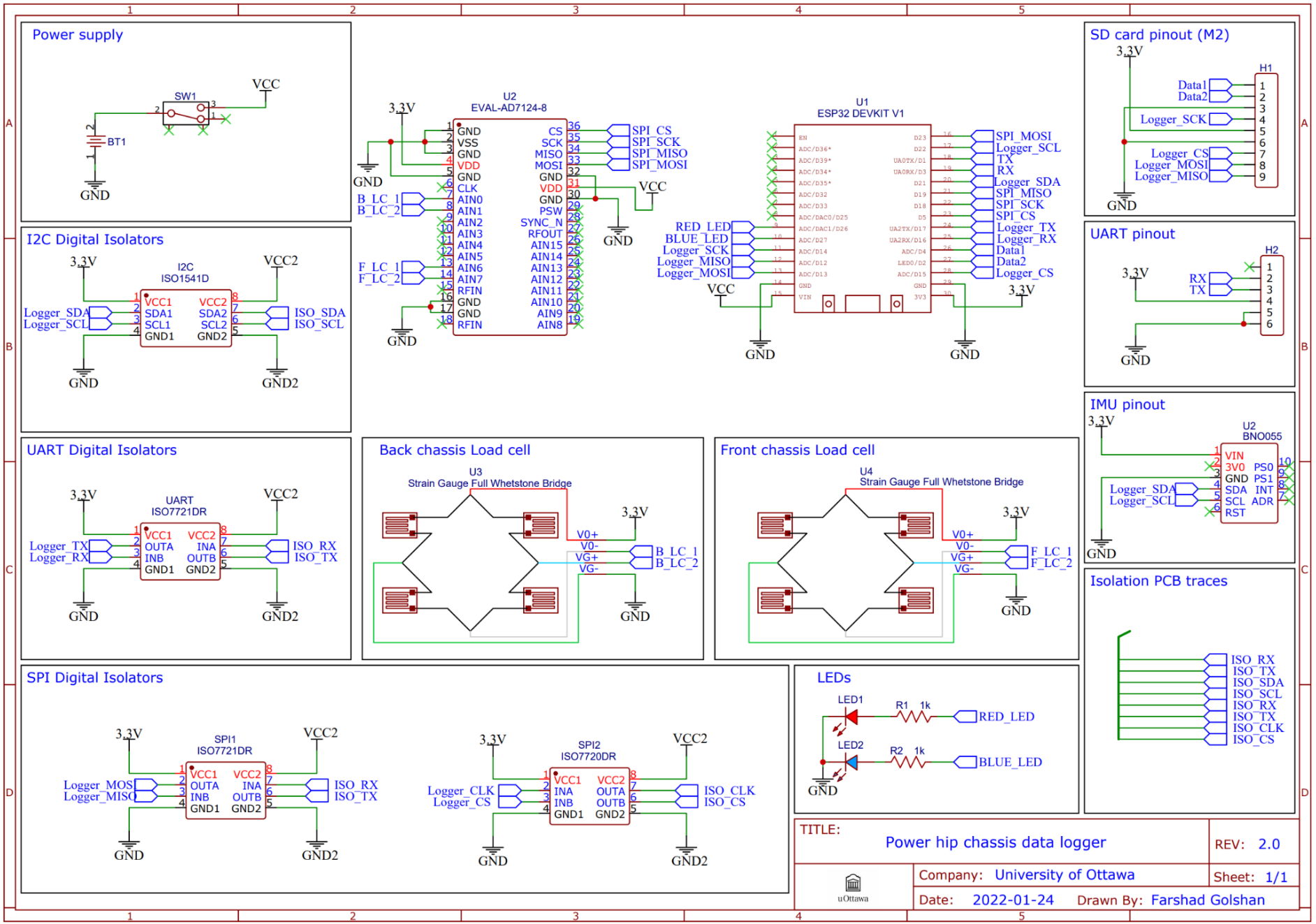

Figure D.1 Detailed diagram of the force measurement electronics system.

Appendix E: Ethics Approval

18/10/2021

Université d'Ottawa
Bureau d'éthique et d'intégrité de la recherche

University of Ottawa
Office of Research Ethics and Integrity

CERTIFICAT D'APPROBATION ÉTHIQUE | CERTIFICATE OF ETHICS APPROVAL

Numéro du dossier / Ethics File Number	H-08-21-7062
Titre du projet / Project Title	DESIGN AND CLINICAL EVALUATION OF AN INTELLIGENT POWERED HIP PROSTHETIC JOINT
Type de projet / Project Type	Recherche de professeur / Professor's research project
Statut du projet / Project Status	Approuvé / Approved
Date d'approbation (jj/mm/aaaa) / Approval Date (dd/mm/yyyy)	18/10/2021
Date d'expiration (jj/mm/aaaa) / Expiry Date (dd/mm/yyyy)	17/10/2022

Équipe de recherche / Research Team

Chercheur / Researcher	Affiliation	Role
Hossein GHOLIZADEH	Département de génie mécanique / Department of Mechanical Engineering	Chercheur Principal / Principal Investigator
Natalie BADDOUR	Département de génie mécanique / Department of Mechanical Engineering	Co-superviseur / Co-supervisor
Michael BOTROS	Département de génie mécanique / Department of Mechanical Engineering	Étudiant-chercheur / Student-researcher
Farshad GOLSHAN	Département de génie mécanique / Department of Mechanical Engineering	Étudiant-chercheur / Student-researcher
Sarah MROZ	Département de génie mécanique / Department of Mechanical Engineering	Étudiant-chercheur / Student-researcher
Edward LEMAIRE	Département de médecine / Department of Medicine	Co-superviseur / Co-supervisor
Yousef BADER	Département de génie mécanique / Department of Mechanical Engineering	Étudiant-chercheur / Student-researcher
Kelly BRANNEN	Département de génie mécanique / Department of Mechanical Engineering	Étudiant-chercheur / Student-researcher

Conditions spéciales ou commentaires / Special conditions or comments

550, rue Cumberland, pièce 154
Ottawa (Ontario) K1N 6N5 Canada

550 Cumberland Street, Room 154
Ottawa, Ontario K1N 6N5 Canada

613-562-5387 • 613-562-5338 • ethique@uOttawa.ca / ethics@uOttawa.ca
www.recherche.uottawa.ca/deontologie | www.recherche.uottawa.ca/ethics

Université d'Ottawa
Bureau d'éthique et d'intégrité de la recherche

University of Ottawa
Office of Research Ethics and Integrity

Le Comité d'éthique de la recherche (CÉR) de l'Université d'Ottawa, opérant conformément à l'*Énoncé de politique des Trois conseils* (2014) et toutes autres lois et tous règlements applicables, a examiné et approuvé la demande d'éthique du projet de recherche ci-nommé.

L'approbation est valide pour la durée indiquée plus haut et est sujette aux conditions énumérées dans la section intitulée "Conditions Spéciales ou Commentaires". Le formulaire « Renouvellement ou Fermeture de Projet » doit être complété quatre semaines avant la date d'échéance indiquée ci-haut afin de demander un renouvellement de cette approbation éthique ou afin de fermer le dossier.

Toutes modifications apportées au projet doivent être approuvées par le CÉR avant leur mise en place, sauf si le participant doit être retiré en raison d'un danger immédiat ou s'il s'agit d'un changement ayant trait à des éléments administratifs ou logistiques du projet. Les chercheurs doivent aviser le CÉR dans les plus brefs délais de tout changement pouvant augmenter le niveau de risque aux participants ou pouvant affecter considérablement le déroulement du projet, rapporter tout évènement imprévu ou indésirable et soumettre toute nouvelle information pouvant nuire à la conduite du projet ou à la sécurité des participants.

The University of Ottawa Research Ethics Board, which operates in accordance with the *Tri-Council Policy Statement* (2014) and other applicable laws and regulations, has examined and approved the ethics application for the above-named research project.

Ethics approval is valid for the period indicated above and is subject to the conditions listed in the section entitled "Special Conditions or Comments". The "Renewal/Project Closure" form must be completedfour weeks before the above-referenced expiry date to request a renewal of this ethics approval or closure of the file.

Any changes made to the project must be approved by the REB before being implemented, except when necessary to remove participants from immediate endangerment or when the modification(s) only pertain to administrative or logistical components of the project. Investigators must also promptly alert the REB of any changes that increase the risk to participant(s), any changes that considerably affect the conduct of the project, all unanticipated and harmful events that occur, and new information that may negatively affect the conduct of the project or the safety of the participant(s).

Kim THOMPSON
Responsable d'éthique en recherche / Protocol Officer
Pour/For **Daniel LAGAREC** Président(e) du/ Chair of the **Comité d'éthique de la recherche en sciences de la santé et sciences / Health Sciences and Sciences Research Ethics Board**

550, rue Cumberland, pièce 154 Ottawa (Ontario) K1N 6N5 Canada
550 Cumberland Street, Room 154 Ottawa, Ontario K1N 6N5 Canada

613-562-5387 • 613-562-5338 • ethique@uOttawa.ca / ethics@uOttawa.ca
www.recherche.uottawa.ca/deontologie | www.recherche.uottawa.ca/ethics